Journal of Molecular Structure 1315 (2024) 138978

Contents lists available at ScienceDirect

Journal of Molecular Structure

journal homepage: www.elsevier.com/locate/molstr

Exploring 2-Pyrazoline derivatives as potent antidiabetic agents and cholinesterase inhibitors: Their synthesis and molecular docking studies

Zefine Uğraş [a], Fatih Tok [b], Cansel Çakir [c], Kübra Tuna [c], Gizem Tatar-Yilmaz [d], Doğukan Mutlu [e], Yusuf Sicak [f], Şevki Arslan [e], Mehmet Öztürk [c], Bedia Koçyiğit-Kaymakçioğlu [a,*]

[a] Department of Pharmaceutical Chemistry, Biruni University, Zeytinburnu, İstanbul 34010, Türkiye,
[b] Department of Pharmaceutical Chemistry, Marmara University, Maltepe, İstanbul 34854, Türkiye
[c] Department of Chemistry, Muğla Sıtkı Koçman University, Kötekli, Muğla 48000, Türkiye
[d] Department of Biostatistics and Medical Informatics, Karadeniz Technical University, Trabzon 81080, Türkiye
[e] Department of Biology, Pamukkale University, Kınıklı, Denizli 20070, Turkey
[f] Department of Herbal and Animal Production, Muğla Sıtkı Koçman University, Kötekli, Muğla 48000, Türkiye

ARTICLE INFO

Keywords:
2-pyrazoline
Synthesis
Antidiabetic
Alzheimer
Docking

ABSTRACT

Herein, unique pyrazoline derivatives were synthesized, and their structures were elucidated by various spectroscopic techniques. Moreover, potential *in vitro* acetylcholinesterase (AChE), butyrylcholinesterase (BChE), α-glucosidase, and α-amylase inhibition effects of the compounds were also investigated. Molecular docking studies were performed to further elucidate the enzyme inhibitory activities. The compound 2c (IC_{50} = 1.64 ±0.04 and 4.18±0.22 μM, respectively) exhibited the strongest inhibitory activity against AChE and BChE, while compounds 2 m (IC_{50} = 4.29±0.20 μM) and 2i (IC_{50} = 4.31±0.08 μM) showed promising AChE inhibitory activity. On the other hand, compounds 2a (IC_{50}= 5.01±0.13 μM) and 2i (IC_{50} = 5.06±0.72 μM) significantly inhibited BChE. In addition, all compounds except 2c and 2f showed great inhibitory activity against α-amylase at lower concentrations compared to acarbose (IC_{50} = 72.57 ± 3.16 μM). Similarly, all compounds except 2k exhibited higher inhibitory activity than acarbose (IC_{50} = 207.08±12.20 μM) against α-glucosidase. Among the compounds, 2a (IC_{50} = 15.05±5.64 μM), 2b (IC_{50} = 14.34±5.05 μM), and 2e (IC_{50} = 11.72±0.46 μM) had excellent inhibitory activity at certain concentrations. The data obtained from the molecular docking studies supported inhibitory activity results. This study presents potential leads for the development of antidiabetic and Alzheimer's therapeutics.

1. Introduction

Heterocyclic compounds carrying nitrogen atoms have always been the focus of attention of researchers due to their diverse and versatile bioactivities [1]. Pyrazolines, for example, have various pharmacological activities such as antidiabetic [2], anticancer [3], anticonvulsant [4], antioxidant [5], antibacterial [6], antipyretic [7], and cholinesterase enzyme inhibition [8]. Currently, numerous studies have been carried out for the synthesis of compounds possessing pyrazoline pharmacophore, especially for the treatment of diabetes and Alzheimer's disease. Saeed et al. synthesized a novel series of pyrazolinyl-acyl thiourea derivatives as potent α-glucosidase and α-amylase inhibitors [9]. A series of 1,3,5-triaryl-2-pyrazoline derivatives which exhibited excellent α-glucosidase inhibitory activity was reported by Mehmood et al. [10]. Machado et al. explored a unique compound bearing pyrazoline scaffold which could be defined as an anti-Alzheimer agent [11]. Unsal-Tan et al. synthesized a series of 2-pyrazoline derivatives as an inhibitor agent against AChE and BChE [12]. Previous studies have demonstrated that the steric and electronic properties of substituents are crucial factors in the design of the compounds. Specifically, the size of the substituents on the aryl group/s and their electron-donating and withdrawing properties play a major role in changing the biological activity [13].

Diabetes caused by unstable blood sugar levels is a common and severe chronic disease worldwide [14]. Diabetes mellitus (DM) is classified as Type I or II based on the amount of insulin produced in cells or secreted by the pancreas [15]. Type II diabetes is more significant because it may be prevented and is more commonly diagnosed, and

* Corresponding author.
E-mail address: bkaymakcioglu@biruni.edu.tr (B. Koçyiğit-Kaymakçioğlu).

https://doi.org/10.1016/j.molstruc.2024.138978
Received 28 February 2024; Received in revised form 8 June 2024; Accepted 10 June 2024
Available online 10 June 2024

caused by an imbalance between the amount of insulin released and the amount of insulin consumed [16]. Type II diabetes mellitus is a multifactorial disease due to a confluence of hereditary and environmental factors, including dietary habits, age, and physical inactivity. The primary strategy to prevent type II diabetes is control of blood sugar, which includes therapeutic approaches such as the reduction of postprandial hyperglycemia, defined as high blood sugar levels due to insufficient insulin production or inadequate response from cells. This could be achieved by inhibiting enzymes responsible for the digestion of carbohydrates localized in intestinal cells, such as α-amylase and α-glucosidase [17]. The α-amylase enzyme is responsible for the digestion of long-chain carbohydrates, while the α-glucosidase enzyme converts starch and disaccharides into glucose. Some commercially available drugs, such as metformin, acarbose, voglibose, and miglitol, were developed based on inhibiting both α-amylase and α-glucosidase [18–20]. Nevertheless, the emergence of side effects like abdominal pain, bloating, diarrhea, and flatulence necessitates the development of new drugs [21]. Therefore, it is necessary to design and synthesize more effective new compounds that provide optimal glycaemic control, enhanced safety profiles, and minimized side effects .

Alzheimer's disease (AD) is a neurodegenerative disorder that impairs neurocognitive function leading to memory loss, cognitive impairment, and a deterioration in language skills [22]. Presently, more than 55 million people worldwide struggle with AD, and the prevalence of the disease is increasing in parallel with the world's aging population [23]. In literature, it is thought that Alzheimer's disease will become a severe public health problem in the coming years with the aging of the world population [24]. While the detailed pathophysiology of Alzheimer's disease remains incompletely understood, it is characterized by progressive degeneration of brain cells, the cause of which is not fully elucidated. Various hypotheses have been proposed to explain its etiology, such as abnormal amyloid β plaque formation (Aβ), tau protein pathology, cholinergic neuron disorder, oxidative stress, and inflammation [25]. Clinical studies have shown that treatments aimed at increasing acetylcholine levels provide symptomatic improvement [26]. Inhibition of acetylcholinesterase (AChE) and butyrylcholinesterase (BChE) is vital in treating cognitive disorders to block the hydrolysis of acetylcholine. Currently, available and notable cholinesterase inhibitors such as donepezil, galantamine, rivastigmine, and tacrine are used to improve the symptoms of Alzheimer's disease [27]. However, these drugs have limited and temporary use and are not effective in preventing or delaying disease progression [28].

Several studies have been conducted in an attempt to define the relationship between diabetes and Alzheimer's disease. While Alzheimer's and Type-2 DM were previously considered two independent metabolic diseases, over time, advances in the study of the pathophysiology of these diseases have revealed that they share many common mechanisms such as insulin resistance, insulin growth factor (IGF) signaling, glycogen synthase kinase 3β signaling mechanism, oxidative stress, and inflammatory response. The formation of Alzheimer's and Type-2 DM diseases has also been associated with mechanisms such as amyloid beta (Aβ) formation, neurofibrillary tangle formation, and regulation of acetylcholine esterase activation. Additionally, epidemiological studies have shown a strong relationship between cognitive impairment and type-2 DM due to impaired glucose absorption in neurons for energy production. As a result, scientists have labeled Alzheimer's as 'Type-3 DM' due to the common mechanisms between these two diseases at the cellular and molecular levels. Activation of neuronal stress signaling pathways is seen as one of the pathological causes of Alzheimer's disease. Given the interconnectedness of Alzheimer's and Type-2 DM, targeting such pathways with antidiabetic agents presents a promising approach. These agents hold potential for treating not only diabetes but also Alzheimer's disease by addressing brain insulin signaling, cognitive impairment, and neurodegeneration [29–32].

Our study aims to examine the multiple biological activity potentials of pyrazoline-based compounds against diabetes and Alzheimer's diseases, which are common worldwide. Specifically, we explored the inhibitory potentials of these compounds against carbohydrate hydrolyzing enzymes (α-glucosidase, α-amylase) and cholinesterase enzymes (acetylcholinesterase, AChE and butyrylcholinesterase, BChE), which play crucial roles in diabetes and Alzheimer's disease, respectively. Molecular features contributing to their effectiveness in the treatment of diabetes and Alzheimer's disease have been revealed through structure-activity relationship analysis. In addition, possible binding modes of compounds with selected targets were evaluated computationally through molecular docking and molecular dynamic simulations.

2. Result and discussion

2.1. Chemistry

In this study, the 4-(4-methylpiperidine)benzaldehyde compound (**1**) was synthesized by reacting 4-methylpiperidine with 4-fluorobenzaldehyde in the presence of K_2CO_3 as a base in dimethylformamide (DMF) under reflux for 10 h (Scheme 1, pathway [I]). Then, compound (**1**) was subjected to a base-mediated Claisen-Schmidt aldol condensation with ketone derivatives in the presence of sodium hydroxide in methanol at room temperature for 12 h to obtain the corresponding chalcones (**1a-1i**) in 77–89% yield (Scheme 1, pathway [II]). In the last step, compounds (**2a-2i**) were synthesized *via* the cyclocondensation of chalcone compounds with phenylhydrazine hydrochloride in ethanol under heating conditions for 10–11 h in the presence of glacial acetic acid, yielding 65–81 % (Scheme 1, pathway [III]). IR, ^{1}H NMR, ^{13}C NMR, and mass spectra were used to elucidate the structures of the achieved compounds. Copies of spectra of the synthesized compounds are provided in supplementary materials as Figures (1–54).

2.2. Spectral data analysis

The IR spectra of the chalcone derivatives (**1a–1i**) revealed the existence of the characteristic carbonyl group (C = O), which is conjugated with an olefinic bond (CH═CH). C = O stretching band of the chalcone derivatives was observed in the 1641–1651 cm^{-1} range. The C = N and C—N stretching bands were observed in the regions in the 1595–1597 cm^{-1} and 1226–1379 cm^{-1}, respectively. The absence of the carbonyl vibration band in the IR spectrum of pyrazoline compounds further supported the formation of the pyrazoline ring.

In ^{1}H NMR spectra of the compounds **1a-1i**, peaks observed in the aromatic and aliphatic regions are consistent with the number and nature of the protons on the scaffold of the corresponding compound. The coupling constant values of olefinic protons of chalcones are observed as either J = 15–16 Hz or J = 7–9 Hz are typical for the *trans* and *cis* configuration about the carbon-carbon double bond, respectively [33]. For instance, the peak at 7.40 ppm (d, J = 15.7 Hz) for compound **1 h** indicates the doublets attributed to unsaturated hydrogens, with the coupling constant (J) confirming *trans* stereochemistry. The pyrazoline ring possesses a unique splitting system known as ABX due to the geminal-vicinal couplings between the non-equivalent methylene protons (Ha and Hb) and the methine proton (Hx), which resonated as a double doublets [34]. The peaks of the Ha, Hb, and Hx protons of the compounds were observed at 2.93–3.14 ppm, 3.74–3.87 ppm, and 5.22–5.49 ppm as double doublets, respectively. The corresponding coupling constants values of these protons were determined to be J_{gem} = 16.9–17.6 Hz, J_{trans} = 5.8–7.0 Hz, and J_{cis} = 12.1–12.6 Hz, respectively. It was determined that the peaks observed in the aliphatic region were suitable for the aliphatic protons of the compounds. Moreover, aromatic protons resonated with compatible integral values in the aromatic region.

In the ^{13}C NMR spectra, the formation of the pyrazoline ring was confirmed by the observation of peaks for the C14, C15, and C16 carbons of the pyrazoline ring in the ranges of 62.28–64.51 ppm, 42.80–43.70 ppm, and 144.28–160.22 ppm, respectively. Additionally, the calculated

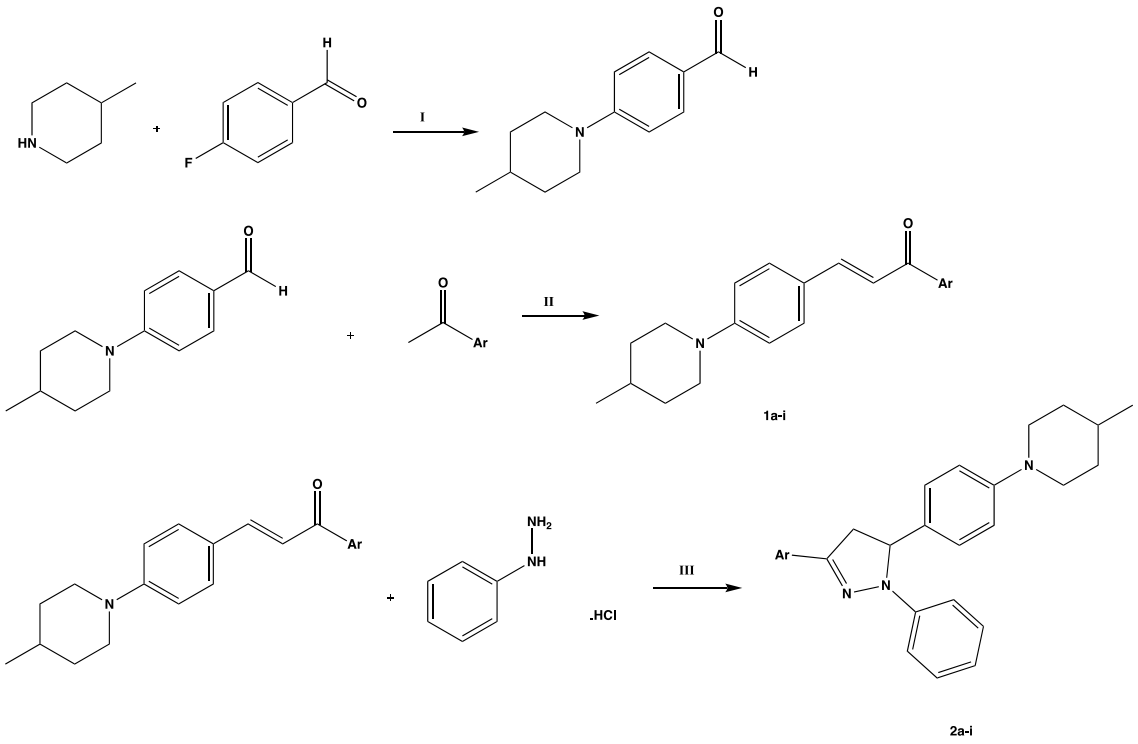

Scheme 1. Synthesis pathways of pyrazoline compounds. ***Reagent and conditions:*** (I) K_2CO_3, DMF, reflux, 10 h; (II) NaOH, methanol, r.t., 12 h; (III) glacial acetic acid, ethanol, reflux, 10–11 h.

m/z values correlate well or compare favorably with the assigned molecular structures.

2.3. Biological activities

2.3.1. Enzyme inhibitory activities

The synthesized compounds were screened/evaluated against *α*-amylase, *α*-glucosidase, acetylcholinesterase, and butyrylcholinesterase at different concentrations (12.5, 25, 50, 100, and 200 μM) in the presence of galantamine and acarbose as positive controls, respectively (Table 1).

2.3.1.1. In vitro α-amylase and α-glucosidase inhibitory activity. All of the synthesized compounds bearing pyrazoline ring except derivatives **2d** and **2f** exhibited more potent activity with IC_{50} values ranging from 28.97±0.80 μM to 42.67±0.73 μM when their amylase inhibitory

Table 1
In vitro α-glucosidase, *α*-amylase, and anticholinesterase inhibitory activities of 2(a-o).[a]

Compound	Ar	α-Amylase Inhibitory Activity IC_{50} (μM)	α-Glucosidase Inhibitory Activity IC_{50} (μM)[b]	Anticholinesterase Inhibitory Activity	
				AChE IC_{50} (μM)[d]	BChE IC_{50} (μM)[d]
2a	4-Chlorophenyl	31.08±1.26[d]	15.05±5.64	6.95±0.64	5.01±0.13
2b	4-Fluorophenyl	39.13±0.67[c]	14.34±5.05	7.21±1.46	7.28±0.37
2c	4-Bromophemyl	42.67±0.73[c]	22.72±5.03	1.64±0.04	4.18±0.22
2d	4-Methylphenyl	112.41±9.20[d]	19.90±0.41	19.87±0.27	24.11±0.95
2e	4-Nitrophenyl	52.48±0.54[d]	11.72±0.46	5.12±0.08	12.84±0.49
2f	4-Cyanophenyl	102.65±1.70[d]	17.17±0.54	9.75±0.17	16.79±0.17
2g	4-Methylthiophenyl	32.98±0.05[c]	21.22±0.26	11.69±0.30	10.07±0.41
2h	5-Methylfuran-2-yl	35.39±1.06[c]	40.11±5.01	12.29±0.61	10.80±0.23
2i	4-Methoxyphenyl	35.37±1.20[c]	116.87±2.29	4.31±0.08	5.06±0.72
2j	-Phenyl	38.20±1.04[c]	140.91±3.68	18.75±0.24	20.66±0.43
2k	5-Chlorothiophen-2-yl	35.49±0.91[c]	*NA*	6.26±0.19	6.24±0.11
2l	Furan-2-yl	42.49±1.27[d]	99.89±1.58	9.80±0.44	10.52±0.38
2m	5-Bromothiophen-2-yl	28.97±0.80[c]	26.42±2.71	4.29±0.20	13.38±0.30
2n	Thiophen-2-yl	31.65±0.18[c]	143.23±0.23	12.12±0.41	5.34±0.04
2o	5-Methylthiophen-2-yl	30.99±0.69[c]	*NA*	13.75±0.59	6.90±0.12
Galantamine[b]		*NT*	*NT*	3.70±0.27	40.20±0.13
Acarbose[b]		72.57 ± 3.16	207.08 ± 12.20	*NT*	*NT*

[a] Values expressed herein are mean ± SEM of three parallel measurements. $p < 0.05$.
NT: not tested.
[b] 25–50–100–200 μM.
[c] 12.5–25–50–100 μM.
[d] 50–100–200–400 μM
‡12.5–25–50–100 mM
IC_{50}: Half maximal inhibitory concentration.

activities were compared to acarbose (IC_{50} = 72.57 ± 3.16 μM).

Except **2k,** the pyrazoline derivatives exhibited increased activity against α-glucosidase compared to acarbose standard (IC_{50} = 207.08 ±12.20 μM) with IC_{50} values ranging from 11.72±0.46 to 143.23±0.23 μM. Compounds **2a, 2b** and **2e** exhibited higher activity among the compounds, with IC_{50} values of 15.05±5.64, 14.34±5.05 and 11.72 ±0.46 μM, respectively.

The structure-activity relationships (SAR) studies indicated that compounds **2a, 2b, 2c, 2e**, and **2f** substituted with an electron-withdrawing group, such as chlorine, fluorine, bromine, nitro, and cyano, respectively, at the 4th position of the phenyl ring, exhibited stronger inhibitory effect against α-glucosidase. On the contrary, compound **2i** substituted with electron-donating group, like the methoxy, showed a decrease in activity. This suggests that electronic factors play a crucial role in modulating inhibitor potency. Additionally, steric effects may also contribute to these observed changes, although the electronic effects appear to be predominant [35,36].

2.3.2. *In vitro anticholinesterase activity*

The anticholinesterase efficacy of **2a-2o** derivatives was assessed against AChE and BChE, and the results were compared with galantamine, utilized as a positive control. The compounds exhibited considerable inhibitory characteristics on cholinesterase enzymes, which are the essential targets in Alzheimer's therapy. Compound **2c** substituted with bromo was the most active against AChE (IC_{50} = 1.64±0.04) and BChE (IC_{50} = 4.18±0.22 μM) compared to galantamine with IC_{50} values of 3.70±0.27 and 40.20±0.13 μM, respectively. Compounds **2 m** substituted with 5-bromothiophen-2-yl and **2i** substituted with 4-methoxyphenyl also exhibited stronger AChE inhibitory activity compared to the other compounds with IC_{50} = 4.29±0.20 and 4.31 ±0.08 μM, respectively. On the other hand, the compounds **2a** and **2i** showed excellent BChE enzyme inhibitory activity with IC_{50} values of 5.01±0.13 and 5.06±0.72 μM, respectively.

When the inhibitory activities of compounds with substitution at the 4th position of the phenyl rings were compared, it was observed a decline in inhibitory activity as the electronegativity of the halogens substituted on the phenyl ring decreased. Further, compound **2c** with bromine at the 4th position of the phenyl ring was found to have the most effective cholinesterase enzyme inhibition.

Replacement of the phenyl ring with a heteroaryl ring carrying an electronegative atom resulted in increased activity. Compound **2l** (IC_{50} = 9.80±0.44 μM, 10.52±0.38 μM, respectively) and **2n** (IC_{50} = 12.12 ±0.41 μM, 5.34±0.04 μM, respectively) showed more potent AChE and BChE inhibitory activity than the compound **2j** (IC_{50} = 18.75±0.24 μM, 20.66±0.43 μM, respectively).

2.3.3. *Cytotoxicity of pyrazoline compounds on L929 cells*

The toxicity of the pyrazolines was performed using the MTT assay against mouse fibroblast cell lines (L929). Table 2 shows the results. All synthesized compounds were found to show no toxic effect against L929 cells, except for compound 2 h (IC_{50} = 247.563 μM), compared to negative control. Only compound **2 h** and paclitaxel reduced the proliferation of the cells by up to 50 % when tested at 250 μM and 10 μg/mL, respectively.

Table 2
Cytotoxicity of the pyrazoline compounds **2(a-o)**[a].

Compound	Ar	IC_{50} (μM)
2a	4-Chlorophenyl	NS
2b	4-Fluorophenyl	NS
2c	4-Bromophemyl	NS
2d	4-Methylphenyl	NS
2e	4-Nitrophenyl	NS
2f	4-Cyanophenyl	NS
2g	4-Methylthiophenyl	NS
2h	5-Methylfuran-2-yl	247.563±1.413[b]
2i	4-Methoxyphenyl	NS
2j	-Phenyl	NS
2k	5-Chlorothiophen-2-yl	NS
2l	Furan-2-yl	NS
2m	5-Bromothiophen-2-yl	NS
2n	Thiophen-2-yl	NS
2o	5-Methylthiophen-2-yl	NS
Paclitaxel [b]		8.40±0.16

[a] Values expressed herein are mean ± SEM of three parallel measurements. $p < 0.05$.
NS: Not showed any cytotoxic effect on applied doses.
[b] 5.6–31.25–62.5–125–250 μM.

2.4. *ADME properties prediction*

Absorption, distribution, metabolism, and elimination (ADME) properties are essential in the development of potential drug candidates. The SwissADME program is widely used to calculate the pharmacokinetic and physicochemical parameters of synthetic molecules [37]. In this study, Lipinski and Veber's rules, which define the ADME properties and physicochemical properties responsible for the transition of the compounds through the blood-brain barrier system, were applied using SwissADME. Analysis of the BOILD-Egg graph revealed that all synthesized pyrazoline compounds successfully penetrated the blood-brain barrier system, indicating their potential for biological activity (Fig. 1).

Physicochemical calculations such as molecular weight (MW), lipophilicity (LogP), hydrogen bond donor number (HBD), hydrogen bond acceptor number (HBA), rotation bond number (RB), and topological polar surface area (TPSA) were also assessed. Compounds were then evaluated for drug-like properties according to their compliance with the Lipinski and Veber rules. Specifically, Lipinski rules include criteria such as MW ≤ 500, LogP ≤ 4.15, HBA ≤ 10, and HBD ≤ 5, while Veber rules entail criteria such as RB ≤ 10 and TPSA ≤ 140 [38,39]. It was found that all compounds evaluated for biological activities complied with the criteria outlined in both Lipinski and Veber rules, as determined by the analysis of ADME and physicochemical parameters using the SwissADME tool [40]. Results from the SwissADME program for the compounds are given in Table 3.

2.5. *Molecular docking analysis*

Molecular docking is a structure-based drug design technique that aims to forecast the binding orientation and binding strength of a particular compound within a designated target protein. The docking score with the lowest binding energy demonstrates that the compound has a higher binding affinity to the protein.

In line with this information, according to the docking analysis, the molecular docking investigation of α-amylase and α-glucosidase enzymes indicated that the binding energy of the reference compound (acarbose) was −6.30 and −4.66 kcal/mol, respectively. All the synthesis compounds exhibited stronger binding affinities within the binding energies range of −9.18 kcal/mol to −7.70 kcal/mol against α-amylase and −8.08 kcal/mol to −7.12 kcal/mol against α-glucosidase than positive compound of acarbose. *In vitro* analysis revealed that compounds **2a, 2b,** and **2e,** which were the most active among the tested compounds, exhibited inhibitory activity at concentrations of 15.05±5.64, 14.34±5.05, and 11.72±0.46 μM against α-glucosidase, respectively. By this, the *in silico* molecular docking studies indicated that these active compounds established bonds with Arg411, Asp616, and Gly651 through hydrogen bonds while interacting with Trp376, Leu678, Leu677, and Leu 650 via pi-alkyl and pi-pi T-shaped bonds (Fig. 2). Specifically, compound **2a** established bonds with Leu678 and Trp376 *via* phenyl moieties. Compound **2b** interacted with Gly651 *via* fluoro atom, while compound **2e** showed interactions with Arg451 and Trp375 *via* nitro group and phenyl ring, respectively. In conclusion, compounds **2a, 2b**, and **2e** exhibited various interactions with specific amino acid residues of the α-glucosidase enzyme. For instance, the aliphatic part of the piperidine ring of the mentioned compounds formed

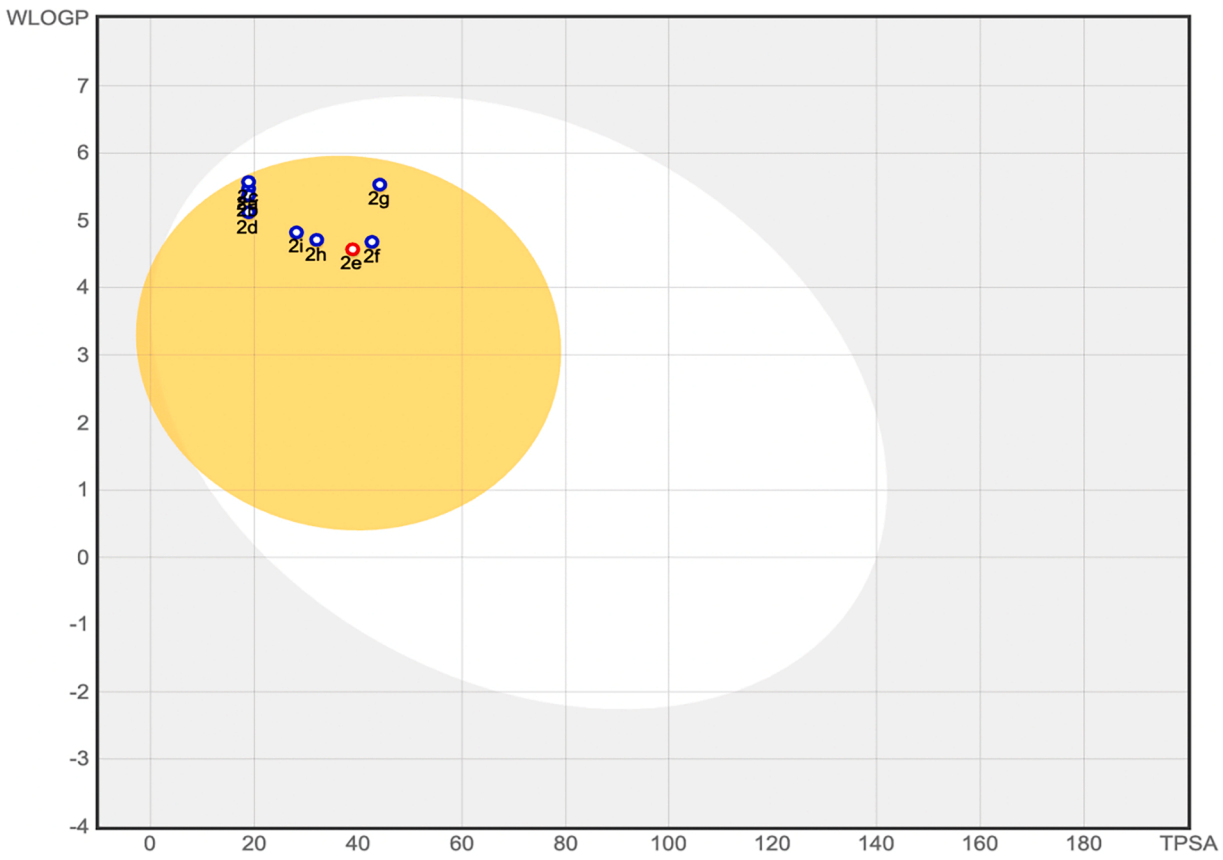

Fig. 1. BOILED-Egg graph of the synthesized compounds.

Table 3
ADME and physicochemical parameters of the compounds.

Molecule	MW	#Rotatable bonds	#H-bond acceptors	#H-bond donors	TPSA	MLOGP	Log S	GI absorption	BBB permeant	Pgp substrate
2a	429.98	4	1	0	18.84	5.58	−7.12	High	Yes	Yes
2b	413.53	4	2	0	18.84	5.48	−6.68	High	Yes	Yes
2c	474.44	4	1	0	18.84	5.67	−7.43	High	Yes	Yes
2d	409.57	4	1	0	18.84	5.31	−6.82	High	Yes	Yes
2e	440.54	5	3	0	38.92	4.10	−6.59	High	Yes	No
2f	420.55	4	2	0	42.63	4.38	−6.47	High	Yes	Yes
2g	441.63	5	1	0	44.14	5.58	−7.04	High	Yes	Yes
2h	399.53	4	2	0	31.98	4.09	−6.40	High	Yes	Yes
2i	425.57	5	2	0	28.07	4.72	−6.60	High	Yes	Yes
2j	395.54	4	1	0	18.84	5.11	−6.52	High	Yes	Yes
2k	436.01	4	1	0	47.08	5.21	−7.36	High	Yes	Yes
2l	385.50	4	2	0	31.98	3.89	−6.07	High	Yes	Yes
2m	480.46	4	1	0	47.08	5.31	−7.68	High	Yes	Yes
2n	401.57	4	1	0	47.08	4.74	−6.56	High	Yes	Yes
2o	415.59	4	1	0	47.08	4.94	−6.88	High	Yes	Yes

alkyl and pi-alkyl interactions with residues such as Trp613, Phe649, Trp516, and His674. Additionally, the phenyl rings of these compounds interacted with other residues like Leu678, Trp376, and Leu677, demonstrating pi-pi T-shaped, alkyl, and pi-alkyl interactions. Commonly, the pyrazoline ring of all three compounds engaged in alkyl and pi-alkyl interactions with specific amino acid residues such as Leu678. As a result, docking studies have shown that pi-pi T-shaped, alkyl, and pi-alkyl interactions play a significant role in the binding process of synthesized compounds with the α-glucosidase enzyme. Particularly, the importance of these interactions in compounds containing electron-withdrawing groups suggests that electron-withdrawing groups may enhance these interactions by reducing the electron density on the structure. Therefore, it has been concluded that electron-withdrawing groups play a crucial role in biological activity.

Moreover, all synthesis compounds demonstrated similar binding affinities against α-amylase with binding energies ranging from −9.18 kcal/mol to −7.70 kcal/mol. Among these compounds, it was compound **2f** that displayed the most favorable binding affinity for α-amylase, with the lowest binding energy of −9.18 kcal/mol. The compound exhibited hydrogen bond interactions with residues Asn105 and Ala106 *via* the cyano group, pi-alkyl bond interactions with Leu162, Leu165, Ala198, and His201 *via* the 4-methyl piperidine, and pi-pi stacked bond interaction with Trp59 *via* the phenyl moeity in α-amylase (Fig. 2). It is worth mentioning that the amino acids responsible for these interactions during the molecular docking process are compatible with interaction sites previously reported in the literature [41,42].

In addition, compounds **2a-2o** demonstrated high effectiveness with binding energies ranging from −12.59 kcal/mol to −9.68 kcal/mol

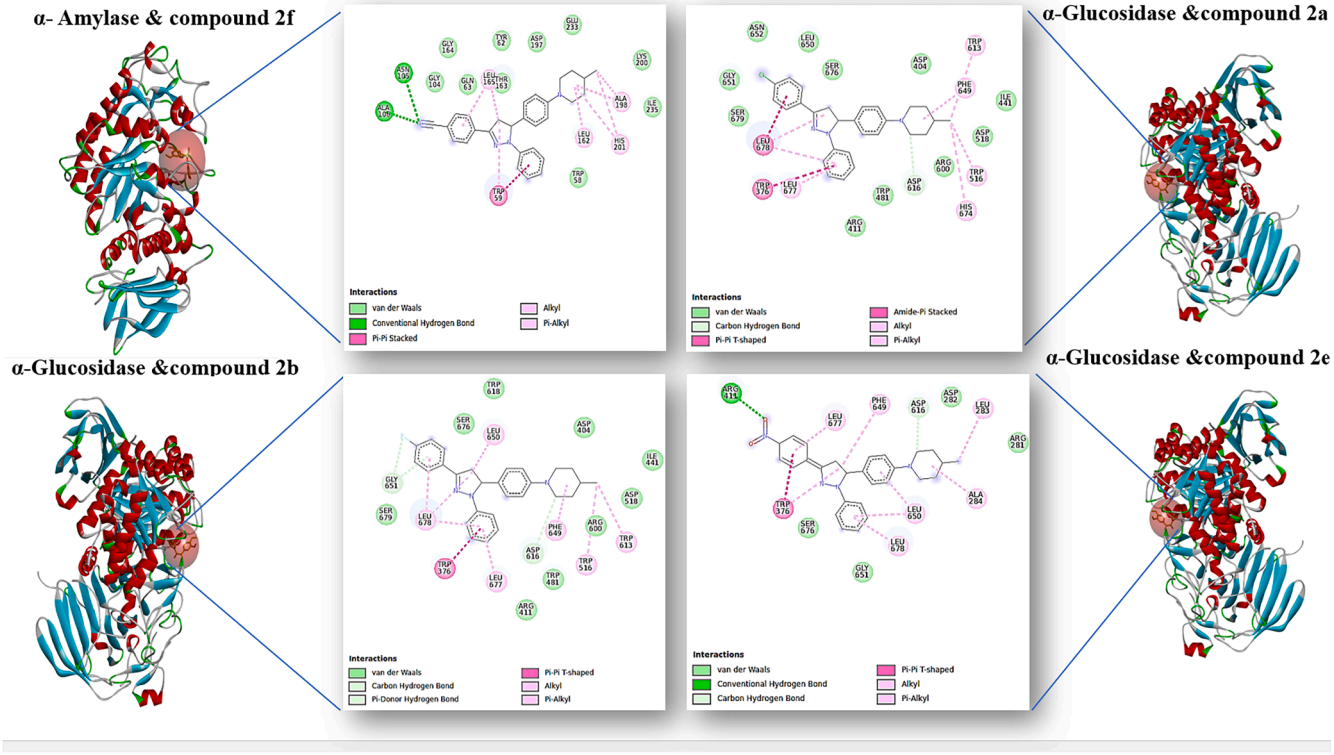

Fig. 2. The 2D analysis of the most active compounds against α-amylase and α-glucosidase enzyme.

against AChE and −10.87 kcal/mol to −8.99 kcal/mol against BChE, in comparison to the positive control, galantamine (Table 4). Compound **2f** demonstrated the most favorable binding affinity with the lowest binding energy of −12.59 kcal/mol against AChE. In addition, compounds **2c, 2i,** and **2 m**, which was the most active compound, exhibited more vital AChE inhibitor activity at 1.64±0.04, 4.31±0.08 and 4.29 ±0.20 μM inhibitory concentrations than galantamine (IC_{50} = 3.70 ±0.27 μM) as given in Table 1. Similarly, these compounds exhibited a significantly higher binding affinity towards AChE than the positive control galantamine *in silico* molecular docking analysis, with a binding energy of −11.15 kcal/mol, −11.34 kcal/mol and −11.35 kcal/mol, respectively.

Table 4
The lowest binding energy values of the compounds **2a-2o** and reference compounds from each docking analysis in the active site of AChE, BChE α-Amylase, and α-Glucosidase.

Compound Number	AChE Binding Energy (kcal/mol)	BChE Binding Energy (kcal/mol)	α-Amylase Binding Energy (kcal/mol)	α-Glucosidase Binding Energy (kcal/mol)
2a	−11.62	−9.93	−8.43	−7.98
2b	−11.31	−9.62	−7.90	−7.52
2c	−11.15	−10.06	−8.72	−7.90
2d	−11.71	−9.73	−8.33	−7.36
2e	−10.03	−10.30	−8.88	−7.12
2f	−12.59	−10.87	−9.18	−8.01
2g	−9.68	−10.12	−8.62	−8.01
2h	−10.93	−9.40	−7.91	−7.94
2i	−11.34	−10.04	−8.31	−7.84
2j	−11.49	−9.45	−7.95	−7.62
2k	−11.59	−9.84	−8.36	−7.85
2l	−11.11	−10.15	−7.70	−7.86
2m	−11.35	−10.02	−8.57	−8.08
2n	−11.64	−8.99	−7.93	−7.45
2o	−11.31	−9.54	−8.11	−7.32
Reference Compounds	−9.13[a]	−7.61[a]	−6.30[b]	−4.66[b]

[a] Galantamine.
[b] Acarbose;.

The critical catalytic functional site of human AChE comprises the catalytic triad, which includes Glu334, His447, and Ser203, as well as the anionic subsite consisting of Trp86, Tyr337, and Phe338. Additionally, there is a peripheral anionic site featuring Tyr72, Trp286, and Tyr341 [43,44]. Compounds **2c, 2i,** and **2 m,** the most active among the series, exhibited non-covalent bonding interactions with these residues, essential in the catalytic functional site of human AChE. Also, these active compounds displayed hydrogen bond interactions with Pro88, Gly120, Tyr133, Glu202, and Ser203 residues in the AChE enzyme. Specifically, compound **2c** contains a bromine atom, interacting with Trp117, Try133, Glu202, and Ile451. Compound **2 m** interacts with Ser125 *via* the sulfur atom in the thiophene ring, and with Pro88 *via* the bromine attached to the thiophene ring. Compound **2i** interacts with Gly120, Tyr133, Glu202, Ile451, Tyr117, and Ser203 *via* the methoxy group attached to the phenyl moiety. In conclusion, the phenyl rings of the three compounds formed pi-pi T-shaped interactions with the Trp86, Tyr337, and Phe338 amino acid residues located in the anionic site of the enzyme. Furthermore, the aliphatic site of the piperidine rings in these compounds interacted with common enzymes to form alkyl and pi-alkyl bonds. Electronegative atoms have played a role in the formation of hydrogen interactions. As a result, the ability of phenyl rings, piperidine, and electronegative atoms to interact with key amino acid residues of the enzyme has played a significant role in the design strategy of these structures. The molecular interactions of the highly active compounds, **2c, 2i,** and **2 m**, with the AChE enzyme, are depicted in Fig. 3, as determined through a combination of *in silico* and *in vitro* studies.

Besides, compounds **2a, 2c,** and **2i** exhibited the most significant BChE enzyme inhibitory activity, with concentrations of 5.01±0.13, 4.18±0.22, and 5.06±0.72 μM, respectively. Also, these compounds showed a strong binding affinity with the lowest binding energy of −9.93, −10.06, and −10.04 kcal/mol against BChE. They were bound to Trp82, Leu125, Tyr128, Ala328, Met437, Trp430, and Trp440 with a pi-

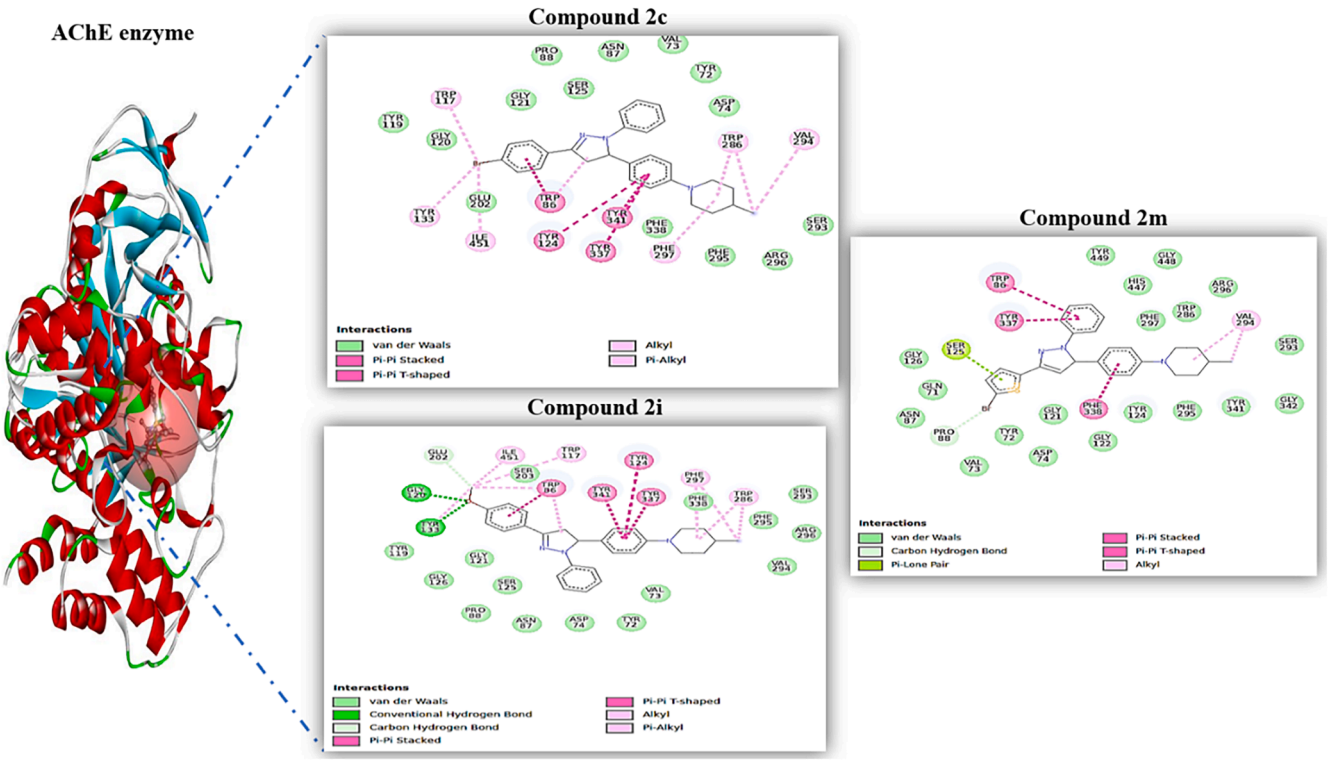

Fig. 3. The 2D analysis of the most active compounds against AChE enzyme with *in silico* and *in vitro* studies.

alkyl bond, Phe329, and Trp231 with pi-pi T-shaped bond as shown in Fig. 4. Further, compound **2a** interacts with Ala277 *via* the chloro atom on the phenyl ring. Compound **2c** interacts with Trp82, Met457, Tyr440, and Trp430 *via* a methoxy group attached to the phenyl ring. Compound **2i** interacts with Asn289 *via* the methoxy group. The catalytic triad within BChE comprises Ser198, His438, and Glu325. Research involving site-directed mutagenesis and affinity studies has confirmed the significance of Trp82 in ligand binding [45,46]. As a result, the phenyl rings of

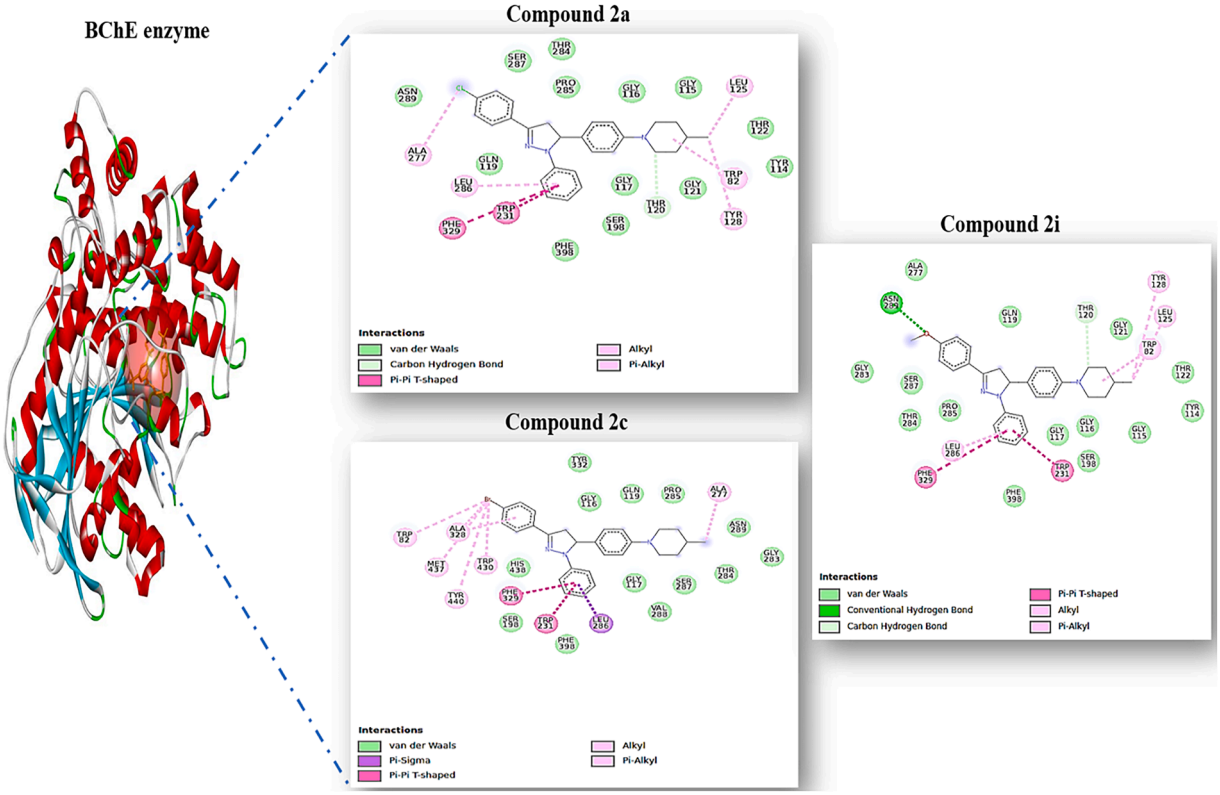

Fig. 4. The 2D analysis of the most active compounds against BChE enzyme with *in silico* and *in vitro* studies.

the three compounds have engaged in alkyl pi-pi T-shaped interactions with the enzyme's Leu286, Phe329, and Trp231 amino acid residues. Additionally, the aliphatic site of the piperidine ring in these compounds has interacted with Leu125 (Compound 2a and 2i), Trp82 (Compound 2a and 2i), Tyr128 (Compound 2a and 2i), and Ala277 (Compound 2c) amino acid residues to form alkyl and pi-alkyl bonds. Electronegative atoms have played a role in hydrogen bonding and pi-alkyl bond formation. Accordingly, the establishment of interactions between phenyl rings, piperidine, and electronegative atoms with crucial amino acid residues of the enzyme underscores their pivotal role in the structural design strategy. The observed binding modes of these compounds within the BChE active site were appropriate, and these interactions play a crucial role in enhancing inhibitor binding affinity.

2.6. Molecular dynamics simulations

In this study, MD simulation was performed using the GROMACS 2020 to investigate the binding stability and dynamics between the compounds identified as the most effective compounds according to the molecular docking results and the target enzymes [47].

The root mean square deviation (RMSD) analysis serves as a valuable tool to assess the stability of the protein-ligand complexes and to identify any significant structural changes or fluctuations that may occur during the MD simulation. In this study, The RMSD analysis was conducted to assess the overall structural stability of the target enzymes with active compounds. The RMSD values ranged from 0.2 to 1.2 nm for all protein-ligand complexes, indicating minimal deviation throughout the 100 ns simulation. Similarly, the RMSD values for the protein and ligand structures exhibited negligible variations, ranging from 0.0005 to 0.5 nm and 0.0004 to 0.2 nm, respectively (as depicted in Fig. 5(A)). These consistent RMSD patterns across the complex, protein, and ligand structures suggest a stable interaction between active compounds and the target proteins. In summary, the RMSD analysis indicates that the reference positions of residues within the active site of target enzymes remained stable over the course of the 100 ns simulation, underscoring the robustness and stability of the interaction between active compounds and target enzymes.

Besides, root mean square fluctuation (RMSF) analysis was employed to examine the fluctuation of target enzymes upon interaction with active compounds. The RMSF analysis revealed fluctuations in the range of 0.04–0.6 nm for the target enzymes (Fig. 5(B)). In addition, we analyzed the radius of gyration (Rg) of the proteins using the molecular

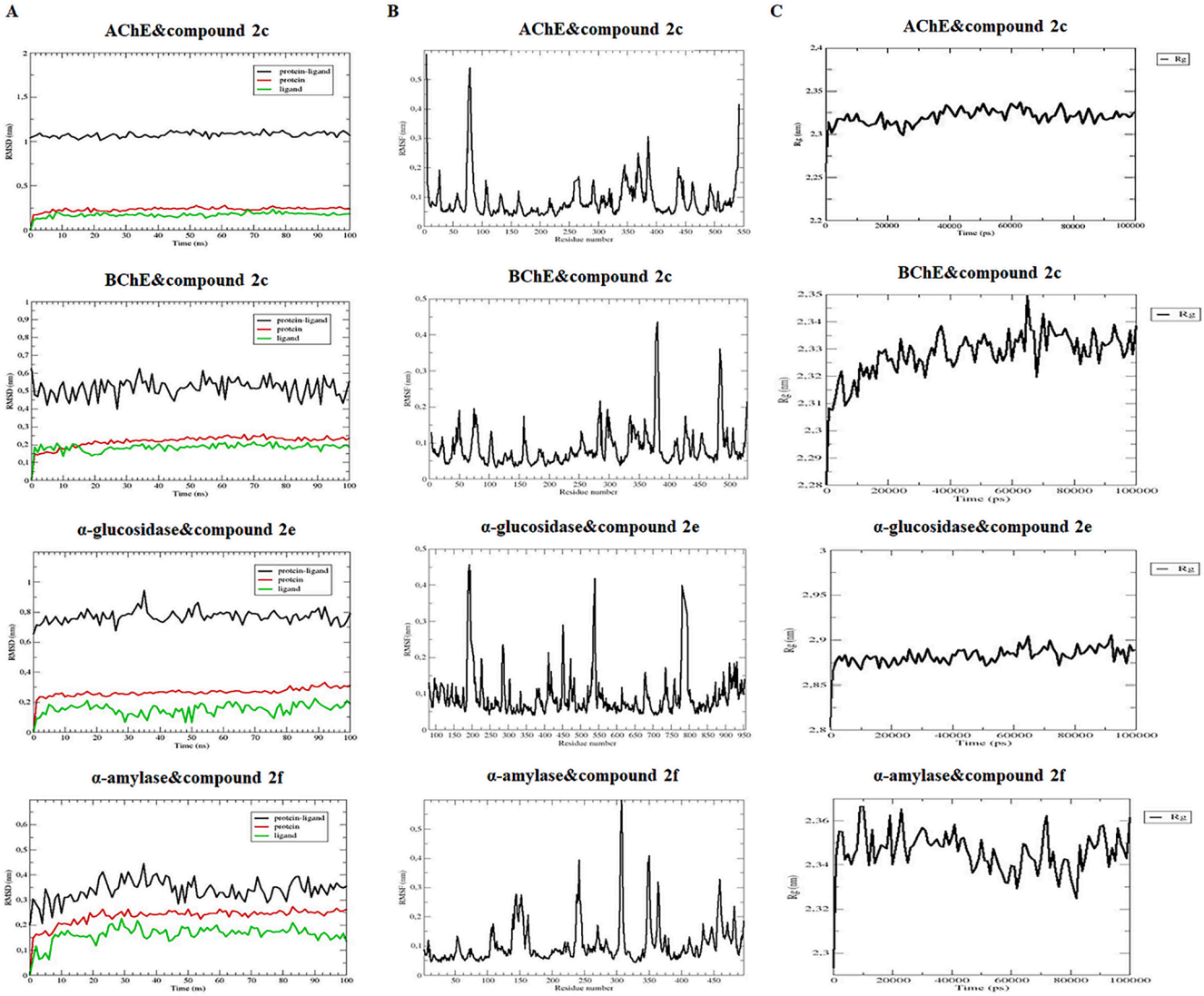

Fig. 5. (A) The RMSD trajectory of protein, ligand, and complex structures. Red color indicates protein, black color indicates complex (protein and ligand), and green color indicates ligand (compound 70) structures. (B) The RMSF profile of target enzymes in the complex structures. (C) Radius of gyration (Rg) analysis of target enzyme structures during the 100 ns MD simulation time.

dynamics simulation data. Rg provides valuable insights into the regular secondary structure and compactness of the target proteins, offering a measure of their overall size and shape. Our observations revealed that Rg values exhibited stable fluctuations between 2.3–2.9 nm for target enzymes during the 100 ns simulation time (Fig. 5(C)). Overall, these analyses provided valuable insights into the dynamic behavior and structural integrity of the target proteins during the molecular dynamics simulation.

Furthermore, in this study, we employed non-covalent 2D interaction diagrams generated using the Discovery Studio program to investigate the detailed intermolecular interactions within the protein-ligand complexes. These diagrams provide visual representations of the specific interactions, including hydrogen bonds, hydrophobic contacts, and electrostatic interactions, between the active site residues of the protein and the ligand. Accordingly, our analysis revealed that interactions with key residues, including Trp286, Tyr341, Tyr72, and Tyr337, located within the critical catalytic functional region of human AChE, remained stable throughout the duration of the MD simulation. These residues are known to play essential roles in the catalytic activity and binding of ligands or inhibitors within the active site of AChE. The stability of interactions with these key residues suggests their significance in maintaining the structural integrity and functional activity of the protein-ligand complex. Similarly, our analysis revealed that non-covalent interactions with the main residues of Ser198, Trp82, Trp231, Leu286, and Val288 located within the active site of the human BChE enzyme, remained stable throughout the molecular dynamics (MD) simulation [48]. In addition, binding site interaction analyses performed for α-glucosidase and α-amylase were observed to be compatible with the interaction regions previously reported in the literature (Fig. 6) [45,46,49].

By analyzing the simulation interaction diagrams, we gained insights into the specific binding modes and key interactions responsible for stabilizing the protein-ligand or protein-inhibitor complexes. This information is invaluable for identifying critical residues involved in ligand binding or inhibitor recognition and guiding the design of novel compounds with improved potency and selectivity.

3. Experimental section

3.1. Chemistry

This study's chemicals, reagents, and solvents were procured from Sigma Aldrich (St. Louis, MO, USA) and Merck (Darmstadt, Germany) and used directly without further purification. Thin-layer chromatography (TLC) employing silica gel (Kieselgel 60, F254) on aluminum sheets from (Merck) was employed to monitor the reaction progress. The solvent system used was a mixture of petroleum ether and ethyl acetate (10:90). Melting points of the synthesized compounds were determined using the Schmelzpunktbestimmer SMP II apparatus. ^{1}H NMR, and ^{13}C NMR, spectra of all compounds were acquired with tetramethylsilane (TMS) as the internal standard, utilizing UXNMR from, Bruker Analytische Messtechnik GmbH (400 Hz), Bruker Avance (300 MHz) and Varian Mercury (Agilent) FT (400 Hz) spectrometers. Nuclear magnetic spectra were recorded using DMSO-d_6 and $CDCl_3$ as solvents. Chemical shift measurements were reported in ppm, while coupling constant values were given in Hertz (Hz). Infrared spectrum (IR) measurements were conducted using the Shimadzu FTIR 8400 S Spectrometer. Mass spectra were obtained using the ESI(+) technique on a Waters ZQ micromass LC-MS spectrometer from Waters Corporation (Milford, MA).

3.1.1. The synthesis procedure of 4-(4-methyl piperidine-1-yl)benzaldehyde

The 4-(4-methylpiperidine-1-yl)benzaldehyde derivative was synthesized using the chemical method described in the literature [50].

3.1.2. The synthesis procedure of chalcone derivatives

The compounds were synthesized according to the synthesis method used in our previous study [51]. In our study, a substituted ketone (1 mmol) and an equivalent amount of benzaldehyde (1 mmol) were reacted with three equivalents of NaOH in methanol at room temperature using a magnetic stirrer to synthesize the appropriate compounds.

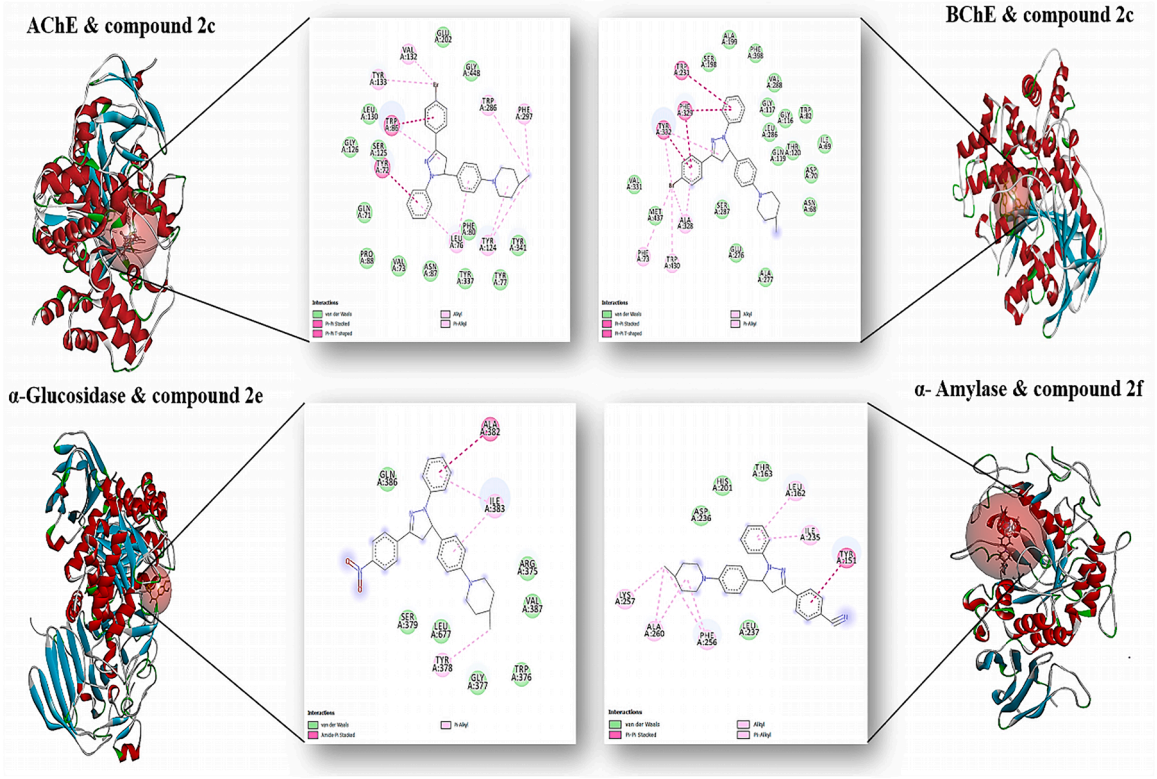

Fig. 6. The 2D interaction analysis of the most active compounds against AChE, BChE, α-amylase, and α-glucosidase enzyme after the 100 ns MD simulation.

The crude compounds were purified by crystallizing ethanol.

3.1.2.1. 1-(4-Chlorophenyl)−3-(4-(4-methyl piperidine-1-yl)phenyl) prop-2-en-1-one (1a). Yield 85 %; m.p. 154.2–154.9 °C; IR ν_{max} = 1651 (C = O); 1581 (chalcone C = C) cm^{-1}; ^{1}H NMR (400 MHz, DMSO-d_6) δ = 0.93 (3H, d, J = 6.4 Hz, CH_3), 1.17 (2H, m, —CH_2-), 1.60 (1H, m, -CH-), 1.69 (2H, m, -CH_2-), 2.82 (2H, m, N—CH_2-), 3.88 (2H, m, N—CH_2-), 7.02 (2H, d, J = 8.5 Hz, Ar), 7.52–7.93 (6H, m, Ar and -CH═CH-), 8.22 (2H, d, J = 8.5 Hz, Ar).

3.1.2.2. 1-(4-Fluorophenyl)−3-(4-(4-methyl piperidine-1-yl)phenyl) prop-2-en-1-one (1b). Yield 80 %; m.p. 132.0–132.6 °C; IR ν_{max} = 1651 (C = O); 1595 (chalcone C = C) cm^{-1}; ^{1}H NMR (400 MHz, DMSO-d_6) δ = 0.93 (3H, d, J = 6.5 Hz, CH_3), 1.17 (2H, q, —CH_2-), 1.59 (1H, m, -CH-), 1.69 (2H, m, -CH_2-), 2.80 (2H, m, N—CH_2-), 3.89 (2H, m, N—CH_2-), 6.97 (2H, d, J = 8.5 Hz, Ar), 7.38 (2H, t, J = 8.7 Hz, Ar), 7.64–7.74 (4H, m, Ar, -CH═CH-), 8.22 (2H, dd, J = 8.5, 5.6 Hz, Ar).

3.1.2.3. 1-(4-Bromophenyl)−3-(4-(4-methyl piperidine-1-yl)phenyl) prop-2-en-1-one (1c). Yield 77 %; m.p. 168.0–168.6 °C; IR ν_{max} = 1645 (C = O g.b.); 1570 (chalcone C = C g.b.) cm^{-1}; ^{1}H NMR (400 MHz, DMSO-d_6) δ = 0.93 (3H, d, J = 6.7 Hz, CH_3), 1.18 (2H, m, —CH_2-), 1.59 (1H, m, -CH-), 1.69 (2H, m, -CH_2-), 2.80 (2H, m, N—CH_2-), 3.89 (2H, m, N—CH_2-), 6.96 (2H, d, J = 8.5 Hz, Ar), 7.19–8.03 (6H, m, Ar, -CH═CH-), 8.07 (2H, d, J = 8.5 Hz, Ar).

3.1.2.4. 3-(4-(4-Methylpiperidin-1-yl)phenyl)−1-(4-methyl phenyl) prop-2-en-1-one (1d). Yield 89 %; m.p. 169.0–169.6 °C; IR ν_{max} = 1651 (C = O); 1581 (chalcone C = C) cm^{-1}; ^{1}H NMR (400 MHz, DMSO-d_6) δ = 0.93 (3H, d, J = 6.5 Hz, CH_3), 1.17 (2H, q, —CH_2-), 1.58 (1H, m, -CH-), 1.68 (2H, m, -CH_2-), 2.42 (3H, s, CH_3), 2.79 (2H, m, N—CH_2-), 3.89 (2H, m, N—CH_2-), 6.96 (2H, d, J = 8.6 Hz, Ar), 7.36 (2H, d, J = 8.0 Hz, Ar), 7.66 (2H, m, Ar, -CH═CH-), 7.70 (2H, d, J = 8.6 Hz, Ar) 8.03 (2H, m, Ar, -CH═CH-).

3.1.2.5. 3-(4-(4-Methyl piperidine-1-yl)phenyl)−1-(4-nitrophenyl)prop-2-en-1-one (1e). Yield 77 %; m.p. 167.0–167.6 °C; IR ν_{max} = 1651 (C = O g.b.); 1568 (chalcone C = C g.b.) cm^{-1}; ^{1}H NMR (400 MHz, DMSO-d_6) δ = 0.93 (3H, d, J = 6.2 Hz, CH_3), 1.18 (2H, m, —CH_2-), 1.62 (1H, m, -CH-), 1.69 (2H, m, -CH_2-), 2.87 (2H, m, N—CH_2-), 3.92 (2H, m, N—CH_2-), 6.50–9.60 (10H, m, Ar, - CH═CH-).

3.1.2.6. 1-(4-Cyanophenyl)−3-(4-(4-methyl piperidine-1-yl)phenyl) prop-2-en-1-one (1f). Yield 77 %; m.p. 175.1–175.6 °C; IR ν_{max} = 2225 (C≡N); 1643 (C = O g.b.); 1566 (chalcone C = C g.b.) cm^{-1}; ^{1}H NMR (400 MHz, DMSO-d_6) δ = 0.90 (3H, d, J = 6.4 Hz, CH_3), 1.16 (2H, m, —CH_2-), 1.59 (1H, m, -CH-), 1.69 (2H, m, -CH_2-), 2.81 (2H, m, N—CH_2-), 3.89 (2H, m, N—CH_2-), 6.49–8.33(10H, m, Ar, -CH═CH-).

3.1.2.7. 3-(4-(4-Methylpiperidin-1-yl)phenyl)−1-(4-(methylthio)phenyl) prop-2-en-1-one (1g). Yield 86 %; m.p. 159.6–161.0 °C; IR ν_{max} = 1647 (C = O); 1577 (chalcone C = C) cm^{-1}; ^{1}H NMR (400 MHz, DMSO-d_6) δ = 0.92 (3H, d, J = 6.5 Hz, CH_3), 1.17 (2H, m, —CH_2-), 1.58 (1H, m, -CH-), 1.68 (2H, m, -CH_2-), 2.56 (3H, s, CH_3), 2.79 (2H, m, N—CH_2-), 3.88 (2H, m, N—CH_2-), 6.97 (2H, d, J = 8.6 Hz, Ar), 7.41 (2H, d, J = 8.5 Hz, Ar), 7.67 (2H, m, Ar, -CH═CH), 7.70 (2H, d, J = 8.6 Hz, Ar) 8.08 (2H, m, Ar, -CH═CH-).

3.1.2.8. 1-(5-Methylfuran-2-yl)−3-(4-(4-methyl piperidine-1-yl)phenyl) prop-2-en-1-one (1h). Yield 87 %; m.p. 189.7–190.3 °C; IR ν_{max} = 1641 (C = O); 1585 (chalcone C = C) cm^{-1}; ^{1}H NMR (400 MHz, DMSO-d_6) δ = 0.93 (3H, d, J = 6.6 Hz, CH_3), 1.18 (2H, d, J = 13.0 Hz, —CH_2-), 1.59 (1H, m, -CH-), 1.69 (2H, d, J = 13.3 Hz, -CH_2-), 2.40 (3H, s, CH_3), 2.79 (2H, t, J = 12.3 Hz, N—CH_2-), 3.88 (2H, d, J = 13.0 Hz, N—CH_2-), 6.41–7.84 (5H, m, Ar, -CH═CH-), 6.96 (2H, d, J = 8.5 Hz, Ar), 7.40 (1H, d, J = 15.7 Hz, -CH═CH-).

3.1.2.9. 1-(4-Methoxyphenyl)−3-(4-(4-methyl piperidine-1-yl)phenyl) prop-2-en-1-one (1i). Yield 89 %; m.p. 145.5–146.1 °C; IR ν_{max} = 1647 (C = O); 1581 (chalcone C = C) cm^{-1}; ^{1}H NMR (400 MHz, DMSO-d_6) δ = 0.93 (3H, d, J = 6.5 Hz, CH_3), 1.19 (2H, m, piperidine —CH_2-), 1.57 (1H, m, -CH-), 1.69 (2H, m, -CH_2-), 2.79 (2H, m, N—CH_2-), 3.87 (5H, m, N—CH_2-, O—CH_3), 6.97 (2H, d, J = 8.4 Hz, Ar), 7.07 (2H, d, J = 8.8 Hz, Ar), 7.59–7.79 (4H, m, Ar, -CH═CH-), 8.22 (2H, dd, J = 8.8, 1.7 Hz, Ar).

3.1.3. The synthesis procedure of 2-pyrazoline derivatives

The current synthetic work extends our previous work, where we reported on synthesis of pyrazoline derivatives (**2j-2o**). The compounds were synthesized according to the synthetic method used in our previous study [50]. In our study, a chalcone derivative (0.01 mol) and phenylhydrazine hydrochloride (0.04 mol) in acetic acid (20 mL) were heated for 10–11 h. The crude solution was poured into ice water. The precipitate was separated by filtration and recrystallized from ethanol [52].

3.1.3.1. 1-(4-(3-(4-Chlorophenyl)−1-phenyl-4,5-dihydro-1H-pyrazole-5-yl)phenyl)−4-methyl piperidine (2a). Yield 73 %; m.p. 162.4–163.0 °C; IR ν_{max} = 1597 (C = N); 1498 (aromatic C = C) cm^{-1}; ^{1}H NMR (400 MHz, DMSO-d_6) δ = 0.91 (3H, d, J = 6.5 Hz, CH_3), 1.18 (2H, d, J = 12.7 Hz, —CH_2-), 1.46 (1H, m, -CH-), 1.65 (2H, d, J = 13.1 Hz, -CH_2-), 2.58 (2H, t, J = 11.9 Hz, N—CH_2-), 3.05 (1H, dd, J_{AB} = 17.6 Hz, J_{AX} = 6.3 Hz, H_A), 3.60 (2H, d, J = 12.4 Hz, N—CH_2-), 3.83 (1H, dd, J_{AB} =17.6 Hz, J_{BX} = 12.2 Hz, H_B), 5.37 (1H, dd, J_{AX} = 6.3 Hz, J_{BX} = 12.2 Hz, H_X), 6.72 (1H, m, Ar), 6.86 (2H, d, J = 8.4 Hz, Ar), 7.01 (2H, d, J = 8.1 Hz, Ar), 7.13 (4H, m, Ar), 7.48 (2H, d, J = 8.3 Hz, Ar), 7.74 (2H, d, J = 8.2 Hz, Ar); ^{13}C NMR (100 MHz, DMSO-d_6) = δ : 22.2, 30.6, 34.0, 43.7, 49.1, 55.7, 63.4, 113.3, 113.5, 114.6, 116.4, 118.5, 119.1, 125.5, 127.0, 127.7, 129.1, 131.8, 132.3, 133.4, 144.5, 145.1, 146.5, 151.0; MS (ESI+) = $C_{27}H_{28}ClN_3$; calcd. m/z = 429.99 [M^+], found m/z = 430.79 [$M + H$]$^+$.

3.1.3.2. 1-(4-(3-(4-Fluorophenyl)−1-phenyl-4,5-dihydro-1H-pyrazole-5-yl)phenyl)−4-methyl piperidine (2b). Yield 77 %; m.p. 132.1–132.7 °C; IR ν_{max} = 1597 (C = N); 1496 (aromatic C = C) cm^{-1}; ^{1}H NMR (400 MHz, DMSO-d_6) δ = 0.92 (3H, d, J = 6.5 Hz, CH_3), 1.18 (2H, d, J = 11.4 Hz, —CH_2-), 1.46 (1H, m, -CH-), 1.66 (2H, d, J = 13.1 Hz, -CH_2-), 2.58 (2H, m, N—CH_2-), 3.07 (1H, dd, J_{AB} = 17.3 Hz, J_{AX} = 6.7 Hz, H_A), 3.61 (2H, d, J = 12.4 Hz, N—CH_2-), 3.83 (1H, dd, J_{AB} = 17.2 Hz, J_{BX} = 12.1 Hz, H_B), 5.36 (1H, dd, J_{AX} = 6.7 Hz, J_{BX} = 12.2 Hz, H_X), 6.71 (1H, m, Ar), 6.88 (2H, d, J = 8.0 Hz, Ar), 7.01 (2H, d, J = 8.0 Hz, Ar), 7.08–7.18 (4H, m, Ar), 7.27 (2H, m, Ar), 7.79 (2H, m; Ar); ^{13}C NMR (100 MHz, DMSO-d_6) = δ 22.2, 30.6, 34.0, 43.5, 49.1, 63.3, 113.4, 116.0, 116.2, 116.5, 118.9, 127.0, 128.2, 128.2, 129.3, 129.6, 132.4, 144.8, 147.8, 151.0; MS (ESI+) = $C_{27}H_{28}FN_3$; calcd. m/z = 413.54 [M^+], found m/z = 414.77 [$M + H$]$^+$.

3.1.3.3. 1-(4-(3-(4-Bromophenyl)−1-phenyl-4,5-dihydro-1H-pyrazole-5-yl)phenyl)−4-methyl piperidine (2c). Yield 81 %; m.p. 166.8–167.4 °C; IR ν_{max} = 1597 (C = N); 1498 (aromatic C = C) cm^{-1}; ^{1}H NMR (400 MHz, DMSO-d_6) δ = 0.92 (3H, d, J = 6.5 Hz, CH_3), 1.17 (2H, d, J = 11.9 Hz, —CH_2-), 1.46 (1H, m, -CH-), 1.66 (2H, d, J = 13.2 Hz, -CH_2-), 2.41–2.70 (2H, m, N—CH_2-), 3.06 (1H, dd, J_{AB} = 17.6 Hz, J_{AX} = 6.3 Hz, H_A), 3.61 (2H, d, J = 12.5 Hz, N—CH_2-), 3.84 (1H, dd, J_{AB} = 17.5 Hz, J_{BX} = 12.5 Hz, H_B), 5.39 (1H, dd, J_{AX} = 6.3 Hz, J_{BX} = 12.5 Hz, H_X), 6.72 (1H, m, Ar), 6.88 (2H, d, J = 8.0 Hz, Ar), 7.02 (2H, d, J = 8.1 Hz, Ar), 7.09–7.15 (4H, m, Ar), 7.63 (2H, d, J = 8.0 Hz, Ar), 7.69 (2H, d, J = 8.5 Hz, Ar); ^{13}C NMR (100 MHz, DMSO-d_6) = δ 22.2, 30.7, 34.0, 43.2, 49.1, 63.3, 113.5, 116.5, 119.1, 122.1, 127.0, 128.0, 129.3, 132.1, 132.2, 132.3, 144.5, 146.6, 151.1; MS (ESI+) = $C_{27}H_{28}BrN_3$; calcd. m/z = 473.15 [M^+], found m/z = 474.77 [$M + H$]$^+$, 476.76 [M + 2H]$^+$.

3.1.3.4. 4-Methyl-1-(4-(3-(4-(methyl phenyl)−1-phenyl-4,5-dihydro-1H-pyrazole-5-yl)phenyl)piperidine (2d). Yield 70 %; m.p. 168.9–169.5 °C; IR ν_{max} = 1597 (C = N); 1496 (aromatic C = C) cm^{-1}; ^1H NMR (400 MHz, DMSO-d_6) δ = 0.92 (3H, d, J = 6.6 Hz, CH_3), 1.19 (2H, m, —CH_2-), 1.47 (1H, m, -CH-), 1.66 (2H, d, J = 13.0 Hz, -CH_2-), 2.34 (1H, s, CH_3), 3.04 (1H, dd, J_{AB} = 17,7 Hz, J_{AX} = 6,2 Hz, H_A), 3.60 (2H, d, J = 13.0 Hz, N—CH_2-), 3.83 (1H, dd, J_{AB} = 17.6 Hz, J_{BX} = 12.1 Hz, H_B), 5.33 (1H, dd, J_{AX} = 6.2 Hz, J_{BX} = 12.1 Hz, H_X), 6.69–6.89 (3H, m, Ar), 7.0 (2H, d, J = 8.1 Hz, Ar), 7.13 (4H, m, Ar), 7.24 (2H, d, J = 7.7 Hz, Ar), 7.64 (2H, d, J = 8.2 Hz, Ar); MS (ESI+) = $C_{28}H_{31}N_3$; calcd. m/z = 409.58 [M^+], found m/z = 410.83 $[M + H]^+$.

3.1.3.5. 4-Methyl-1-(4-(3-(4-nitrophenyl)−1-phenyl-4,5-dihydro-1H-pyrazole-5-yl)phenyl)-piperidine (2e). Yield 80 %; m.p. 188.8–197.4 °C; IR ν_{max} = 1593 (C = N); 1498 (aromatic C = C) cm^{-1}; ^1H NMR (400 MHz, $CDCl_3$) δ = 0.98 (3H, d, J = 6.0 Hz, CH_3), 1.29–1.73 (5H, m, -CH_2-), 2.41–2.70 (2H, m, N—CH_2-), 3.14 (1H, dd, J_{AB} = 16.9 Hz, J_{AX} = 7.0 Hz, H_A), 3.62 (2H, m, N—CH_2-), 3.82 (1H, dd, J_{AB} = 16.9 Hz, J_{BX} = 12.6 Hz, H_B), 5.35 (1H, dd, J_{AX} = 7.0 Hz, J_{BX} = 12.6 Hz, H_X), 6.65–8.45 (13H, m, Ar); ^{13}C NMR (100 MHz, $CDCl_3$) = δ 21.7, 30.5, 34.0, 42.8, 49.9, 64.5, 113.9, 116.7, 120.2, 124.0, 125.8, 126.7, 129.0, 143.9, 146.9; MS (ESI+) = $C_{27}H_{28}N_4O_2$; calcd. m/z = 440.22 [M^+], found m/z = 441.05 $[M + H]^+$.

3.1.3.6. 1-(4-(3-(4-Cyanophenyl)−1-phenyl-4,5-dihydro-1H-pyrazole-5-yl)phenyl)−4-methyl piperidine (2f). Yield 80 %; m.p. 188.8–197.4 °C; IR ν_{max} = 2224 (C≡N); 1597 (C = N); 1494 (aromatic C = C) cm^{-1}; ^1H NMR (400 MHz, DMSO-d_6) δ = 0.91 (3H, d, J = 6.5 Hz, CH_3), 1.21 (2H, m, —CH_2-), 1.48 (1H, m, -CH-), 1.67 (2H, d, J = 13.4 Hz, -CH_2-), 2.63 (2H, t, J = 13.8 Hz, N—CH_2-), 3.10 (1H, dd, J_{AB} = 17.6 Hz, J_{AX} = 6.1 Hz, H_A), 3.59 (2H, m, N—CH_2-), 3.86 (1H, dd, J_{AB} = 17.6 Hz, J_{BX} = 12.5 Hz, H_B), 5.49 (1H, dd, J_{AX} = 6.1 Hz, J_{BX} = 12.5 Hz, H_X), 6.70–8.03 (13H, m, Ar); ^{13}C NMR (100 MHz, $CDCl_3$) = δ 21.8, 30.6, 34.0, 42.8, 49.6, 64.4, 110.9, 113.8, 116.7, 119.0, 119.9, 125.8, 126.6, 126.6, 129.0, 132.3, 137.3, 143.9, 144.28; MS (ESI+) = $C_{28}H_{28}BrN_4$; calcd. m/z = 420.23 [M^+], found m/z = 421.10 $[M + H]^+$.

3.1.3.7. 4-Methyl-1-(4-(3-(4-(methylthio)phenyl)−1-phenyl-4,5-dihydro-1H-pyrazole-5-yl)phenyl)piperidine (2g). Yield 73 %; m.p. 193.3–193.9 °C; IR ν_{max} = 1597 (C = N); 1489 (aromatic C = C) cm^{-1}; ^1H NMR (400 MHz, DMSO-d_6) δ = 0.94 (3H, d, J = 6.1 Hz, CH_3), 1.33–1,75 (5H, m, —CH_2-, -CH-), 2.45–2.78 (5H, m, N—CH_2-, S-CH_3), 3.06 (1H, dd, J_{AB} = 17.4 Hz, J_{AX} = 6.2 Hz, H_A), 3.70 (2H, m, N—CH_2-), 3.87 (1H, dd, J_{AB} = 17.4 Hz, J_{BX} = 12.1 Hz, H_B), 5.45 (1H, dd, J_{AX} = 6.2 Hz, J_{BX} = 12.1 Hz, H_X), 6.71–7.83 (13H, m, Ar); ^{13}C NMR (100 MHz, DMSO-d_6) = δ 14.9, 22.1, 29.4, 32.9, 33.5, 43.3, 62.9, 113.3, 113.6, 115.6, 119.0, 125.3, 126.1 126.3, 126.4, 126.6, 127.4, 128.1, 129.2, 129.4, 129.5, 129.7, 130.0, 139.6, 144.6, 147.4, 150.8; MS (ESI+) = $C_{28}H_{31}N_3S$; calcd. m/z = 441.64 [M^+], found m/z = 442.82 $[M + H]^+$.

3.1.3.8. 1-[4-(1-Phenyl-3-(5-methyl-furan-2-yl)−4,5-dihydro-1H-pyrazole-5-yl)phenyl]−4-methyl piperidine (2h). Yield 65 %; m.p. 114.7–115.3 °C; IR ν_{max} = 1595 (C = N); 1498 (aromatic C = C) cm^{-1}; ^1H NMR (400 MHz, DMSO-d_6) δ = 0.93 (3H, d, J = 6.5 Hz, CH_3), 1.25 (2H, m, —CH_2-), 1.52 (1H, m, -CH-), 1.69 (2H, m, -CH_2-), 2.36 (3H, s, CH_3), 2.41–2.61 (2H, m, N—CH_2-), 2.93 (1H, dd, J_{AB} = 17.2 Hz, J_{AX} = 5.8 Hz, H_A), 3.58 (2H, d, J = 12.3 Hz, N—CH_2-), 3.75 (1H, dd, J_{AB} = 17.2 Hz, J_{BX} = 12.1 Hz, H_B), 5.36 (1H, dd, J_{AX} = 5.8 Hz, J_{BX} = 12.1 Hz, H_X), 6.23 (1H, d, J = 3.1 Hz, Ar), 6.64 (1H, d, J = 3.1 Hz, Ar), 6.69 (1H, m, Ar), 6.94 (3H, m, Ar), 7.13 (5H, m, Ar); ^{13}C NMR (100 MHz, DMSO-d_6) = δ 13.9, 22.0, 33.5, 43.2, 62.3, 108,7, 112.7, 113.3, 118.8, 127.2, 129.3, 139.7, 144.6, 146.4, 153.9; MS (ESI+) = $C_{26}H_{29}N_3O$; calcd. m/z = 399.54 [M^+], found m/z = 400.78 $[M + H]^+$.

3.1.3.9. 1-(4-(3-(4-Methoxyphenyl)−1-phenyl-4,5-dihydro-1H-pyrazole-5-yl)phenyl)−4-methyl piperidine (2i). Yield 65 %; m.p. 114.7–115.3 °C; IR ν_{max} = 1597 (C = N); 1496 (aromatic C = C) cm^{-1}; ^1H NMR (400 MHz, DMSO-d_6) δ = 0.91 (3H, d, J = 6.5 Hz, CH_3), 1.17 (2H, d, J = 12.7 Hz, —CH_2-), 1.46 (1H, m, -CH-), 1.65 (2H, d, J = 13.1 Hz, -CH_2-), 2.58 (2H, t, J = 12.0 Hz, N—CH_2-), 3.02 (1H, dd, J_{AB} = 17.1 Hz, J_{AX} = 6.1 Hz, H_A), 3.59 (2H, d, J = 11.9 Hz, N—CH_2-), 3.74–3.87 (4H, m, H_B, O—CH_3), 5.28 (1H, dd, J_{AX} = 6.1 Hz, J_{BX} = 12.1 Hz, H_X), 6.68–7.70 (13H, m, Ar); ^{13}C NMR (100 MHz, DMSO-d_6) = δ 22.2, 30.6, 33.9, 34.0, 43.3, 49.2, 55.8, 62.9, 113.2, 114.6, 116.5, 118.5, 125.5, 127.0, 126.3, 127.7, 129.2, 132.6, 145.1, 147.6, 150.9, 160.2; MS (ESI+) = $C_{28}H_{31}N_3O$; calcd. m/z = 425.58 [M^+], found m/z = 426.96 $[M + H]^+$.

3.2. Biological activity

All experiments were performed three times. The reaction was monitored using the DMSO as a negative control. The bleaching rate was established from the absorbance differences towards time. $A_{0.5}$, the concentration corresponding to the 0.500 absorbance for CUPRAC assay, and $IC_{50,}$ the concentration corresponding to the 50 % inhibitory activity for remaining enzymatic activities, were calculated from the graphs of inhibitory% against sample concentrations. All activity measurements were performed on a 96-well microplate reader (SpectraMax 340PC^{384}, Molecular Devices, USA).

3.2.1. In vitro enzyme inhibitory activities

Galantamine for anticholinesterase activity, acarbose for α-amylase, and α-glucosidase inhibitory activities were utilized as reference standards to evaluate the inhibitory activities.

3.2.1.1. Determination of α-glucosidase inhibitory activity of 2a-2o derivatives. The α-glucosidase inhibitory activity of **2a-2o** derivatives was performed according to spectroscopic method with slight adaptations [53]. To outline the process, 25 μL of PNPG (*p*-nitrophenyl-*α*-*d*-glucopyranoside) in phosphate buffer (10 mM pH=6.9), 50 μL of phosphate buffer (10 mM pH=6.9), 10 μL of the sample solution, and 25 μL of the α-glucosidase (0.1 U/mL) in 10 mM phosphate buffer (pH=6.0) were combined in a 96-well microplate. After a 20 min of incubation at 37 °C, 90 μL of sodium carbonate (100 mM) was added into each well. Subsequently, the absorbance was read at 400 nm.

3.2.1.2. Determination of α-amylase inhibitory activity of 2a-2o derivatives. The assessment of α-amylase inhibitory activity for **2a-2o** derivatives underwent scrutiny using a spectroscopic method though minor changes [54]. In summary, 25 μL of varied concentration sample solutions and α-amylase solution (0.1 U/mL, 50 μL) in 20 mM phosphate buffer (pH=6.9 phosphate buffer containing 6 mM NaCl) were added each well. After 10 min of pre-incubation at 37 °C, 0,05 % starch solution (50 μL) was added. Then, to monitor and stop the reaction, 100 μL of Lugol solution and 25 μL of 0,1 M HCl were added, respectively. The reaction was monitored at 565 nm.

3.2.1.3. Determination of anticholinesterase activity of 2a-2o derivatives. The evaluation of anticholinesterase activity in DMSO of **2a-2o** derivatives employed electric eel acetylcholinesterase (AChE, Type-VI-S, EC 3.1.1.7, 425.84 U/mg) and horse reddish butyrylcholinesterase (BChE, EC 3.1.1.8, 11.4 U/mg) The assessment was conducted using spectroscopic methods with acetylthiocholine iodide and butyrylthiocholine chloride as substrates [55]. Initially, a mixture comprising 130 μL sodium phosphate buffer (100 mM, pH 8.0), 10 μL **2a-2o** derivatives at different concentrations, and 20 μL AChE or BChE enzymes in the buffer was prepared. After a 15 min incubation at 25 °C, 20 μL 0.5 mM DTNB (5,5-dithiobis (2-nitrobenzoic acid) and 20 μL either acetylthiocholine iodide (0.71 mM) or butyryl-thiocholine chloride (0.2 mM) were added. Subsequently, the absorbance at 412 nm was

measured.

3.2.2. Cell culture and viability assay

Mouse fibroblast (L929, ECACC) cell line was cultivated in Dulbecco's Modified Eagle Medium (DMEM, Sigma) enriched with 1 % penicillin/streptomycin (Gibco) and 10 % fetal bovine serum (FBS, Gibco) at 37 °C, and 5 % CO_2. Cells were maintained in a 75cm^2 cell culture flask, with the medium changed every 2–3 days. Cells were passaged after they reached 90 % confluency, as described previously [56]. The viability assay was evaluated by using MTT (3-(4,5-dimethyl-2-thiazolyl)−2, 5-diphenyl-2H-tetrazolium bromide) reagent (ROTH). All compounds were dissolved in Dimethyl Sulfoxide (DMSO, Carlo Erba), and the final DMSO concentration did not exceed 0.5 %. Briefly, the cells (2×10^3 cells/well) were plated in a 96-well plate and, after 24 h incubation, treated with different concentrations (15.6, 31.25, 62.5, 125, and 250 μM) of pyrazoline compounds for 24 h. Then, the medium was aspirated, and 10 μL MTT solution (5 mg/mL) in 100 μL fresh medium was added to each well. After 4 h, 50 μL of DMSO was added to dissolve the formazan crystals. Absorbance was measured using a microplate spectrophotometer (Epoch, BioTek) at 590 nm. The 0.5 % DMSO-treated cells were used as negative controls, and 10 μg/mL Paclitaxel (Sigma-Aldrich) was used as the positive control. As described previously, obtained IC_{50} values against fibroblast cells were calculated using GraphPad Prism 9.0 software [57].

3.3. Calculation of ADME and physicochemical parameters

ADME and physicochemical calculations of synthesized compounds were freely performed utilizing the SwissADME website [40].

3.4. Molecular docking studies

This research explored the binding affinities and molecular interaction mechanisms of compounds **2a-2o** concerning AChE, BChE, α-glucosidase, and α-amylase employing the AutoDock 4.2 program [58]. The 3D crystal structures of the targeted four enzymes were procured from the Protein Data Bank website (http://www.rcsb.org/pdb) via their respective PDB IDs: 4EY6, 6QAA, 4W93, and 5NN4, respectively. These crystal structures underwent preparation involving the removal of water and ion molecules, with the addition of suitable hydrogen atoms under physiological pH conditions (pH = 7) utilizing the APBS-PDB2PQR software [59]. The determination of the grid box for docking was based on the binding site location of the crystallized ligands. The docking procedure adhered to standard protocols, utilizing a rigid protein and a flexible ligand, and was executed through 100 generations using the Lamarckian Genetic algorithm. Throughout the analysis, predictions were made for binding free energy (ΔG) and inhibitory constant (K_i) values for all compounds, aiding in identifying those demonstrating the most compatible conformational fit to the 3D structure of the targeted enzymes.

3.5. Molecular dynamics simulation

Molecular dynamics (MD) simulation has emerged as a powerful computational technique for studying the dynamic behavior of protein-ligand complexes at the atomic level. Numerous studies have utilized MD simulations to investigate the structural dynamics, energetics, and binding mechanisms of these complexes, contributing to our understanding of drug discovery and design processes [60]. The simulation setup involves preparing the initial coordinates of the protein-ligand complex, solvating the system with water molecules, and adding counterions to maintain charge neutrality. In line with this information, in this study, molecular dynamics (MD) simulations were conducted using the GROMACS 2020 to explore the binding stability and dynamics of compounds identified as the most effective ligands based on molecular docking results with target enzymes [47]. The ligand topology parameters were obtained using the CGenFF Server, while the protein structure was modeled using the CHARMM36 all-atom force field along with the TIP3P water model [61,62]. Subsequently, the system was enclosed within a dodecahedron box under periodic boundary conditions, and sodium and chlorine ions were introduced to achieve electrical neutrality. Following system preparation, MD simulation was conducted in three stages: energy minimization, equilibration, and production. During the initial energy minimization stage, a gradient descent method comprising 1000 steps was employed to alleviate steric clashes and rectify any inappropriate geometry within the system. Subsequently, the system underwent equilibration under both isochoric-isothermal (NVT) and isothermal-isobaric (NPT) ensembles for 100 ps. Finally, the production stage executed a 100 ns MD simulation with a time step of 2 femtoseconds. In addition, we performed analysis of the molecular dynamics (MD) trajectories, focusing on extracting key structural, energetic, and dynamic properties of the protein-ligand complex. We employed commonly used metrics such as root mean square deviation (RMSD), root mean square fluctuation (RMSF), and radius of gyration (Rg) calculations to assess the structural stability and flexibility of the complex. These analyses provided valuable insights into the conformational changes and dynamic behavior of the protein-ligand interaction throughout the simulation period.

4. Conclusion

The research conducted herein centered on the synthesis and comprehensive elucidations of a novel series of pyrazoline derivatives, and it further explored their inhibitory potentials against key enzymes that play essential roles in Alzheimer's and diabetes mellitus diseases. Several significant findings emerged through a precise analysis of both *in vitro* enzyme inhibitory assays and molecular docking studies.

The results revealed that all evaluated compounds met the criteria outlined in both Lipinski and Veber rules, suggesting their potential suitability for further development as therapeutic agents for diabetes and Alzheimer's disease. Further, the majority of the synthesized compounds exhibited noteworthy inhibitory activity against α-amylase and α-glucosidase enzymes, with some compounds surpassing the potency of the reference standard acarbose (IC_{50} = 72.57 ± 3.16 μM, 207.08 ±12.20 μM, respectively). Compound **2c** demonstrated remarkable inhibitory activity against both acetylcholinesterase (AChE) and butyrylcholinesterase (BChE), with IC_{50} values of 1.64 ± 0.04 and 4.18 ± 0.22 μM, respectively, making it the most potent inhibitor among the tested compounds.

Moreover, the results from cytotoxicity studies showed that, except for compound 2 h, the tested compounds did not exhibit toxic effects on healthy cells. Additionally, the results obtained from the SAR of the compounds are supported by the findings obtained from the molecular docking studies of the compounds and *in vitro* enzyme inhibition assays, providing valuable insights into the molecular features that contribute to the efficacy of these compounds in the potential treatment of diabetes and Alzheimer's disease. Besides, the strategic molecular design approach implemented in this study capitalizes on the specific interactions observed between synthesized compounds and key enzyme residues. Notably, the deliberate placement of functional groups such as electron-withdrawing groups, aromatic rings, and aliphatic motifs highlights their significant role in enhancing binding affinity through various interaction mechanisms.

In conclusion, recent research expands the knowledge base of pyrazoline chemistry and offers promising leads for developing novel therapeutics for diabetes and Alzheimer's disease. The novel pyrazoline derivatives synthesized in this study exhibit significant inhibitory properties against key enzymes associated with these conditions, suggesting their potential as candidates for further investigation and development. This renders them highly appealing for potential commercialization and utilization as targeting drugs in antidiabetic and anti-Alzheimer treatments.

Disclosure statement

No potential conflict of interest was reported by the author(s).

CRediT authorship contribution statement

Zefine Uğraş: Writing – original draft, Visualization, Software, Methodology, Investigation, Formal analysis, Conceptualization. **Fatih Tok:** Writing – review & editing, Visualization, Investigation, Conceptualization. **Cansel Çakir:** Writing – original draft, Software, Methodology, Investigation, Formal analysis, Conceptualization. **Kübra Tuna:** Writing – original draft, Visualization, Software, Investigation, Formal analysis, Conceptualization. **Gizem Tatar-Yilmaz:** Writing – original draft, Visualization, Software, Methodology, Investigation, Formal analysis, Conceptualization. **Doğukan Mutlu:** Writing – original draft, Visualization, Software, Investigation, Formal analysis, Conceptualization. **Yusuf Sicak:** Writing – review & editing, Supervision, Investigation, Conceptualization. **Şevki Arslan:** Supervision, Investigation, Conceptualization. **Mehmet Öztürk:** Writing – review & editing, Supervision, Investigation, Conceptualization. **Bedia Koçyiğit-Kaymakçioğlu:** Writing – review & editing, Visualization, Supervision, Investigation, Conceptualization.

Declaration of competing interest

The authors declare that they have no known competing financial interests or personal relationships that could have appeared to influence the work reported in this paper.

Data availability

No data was used for the research described in the article.

Acknowledgments

This work was supported by the Scientific and Technological Research Council of Turkey (TÜBİTAK) [Grant Number: 221S850]; TUBITAK ULAKBIM; High Performance and Grid Computing Center (TRUBA resources).

Supplementary materials

Supplementary material associated with this article can be found, in the online version, at doi:10.1016/j.molstruc.2024.138978.

References

[1] B. Dash, S Karim, Pyrazoline heterocyclic: a review, Int. J. Pharm. Sci. Res. 12 (5) (2021) 2570–2588, https://doi.org/10.13040/IJPSR.0975-8232.12(5).2570-88.
[2] M. Emayavaramban, N. Santhi, C. Gopi, C. Manivannan, Raguraman A. Synthesis, Characterization and antidiabetic activity of 1,3,5-triaryl-2-pyrazolines in acetic acid solution under ultrasound irradiation, Int. Lett. Chem. Phys. Astron. 14 (2013) 172–185, https://doi.org/10.56431/p-2lhl0m.
[3] F. Tok, B. İrem Abas, Ö. Çevik, B Koçyiğit-Kaymakçıoğlu, Design, synthesis and biological evaluation of some new 2-pyrazoline derivatives as potential anticancer agents, Bioorg. Chem. 102 (2020) 104063, https://doi.org/10.1016/j.bioorg.2020.104063.
[4] Z. Ozdemir, H.B. Kandilci, B. Gümüşel, U. Caliş, A.A. Bilgin, Synthesis and studies on antidepressant and anticonvulsant activities of some 3-(2-furyl)-pyrazoline derivatives, Eur. J. Med. Chem. 42 (3) (2007) 373–379, https://doi.org/10.1016/j.ejmech.2006.09.006.
[5] A. Kumar, V. Bhat, R.K. Singla, Synthesis and evaluation of antioxidant activity of novel 3,5-disubstituted-2-pyrazolines, Bull. Fac. Pharm. Cairo Univ. 51 (2) (2013) 167–173, https://doi.org/10.1016/j.bfopcu.2013.04.002.
[6] M. Rani, M Mohamad, Synthesis, studies and in vitro antibacterial activity of some 5-(thiophene-2-yl)-phenyl pyrazoline derivatives, J. Saudi Chem. Soc. 18 (5) (2014) 411–417, https://doi.org/10.1016/j.jscs.2011.09.002.
[7] F. Manna, F. Chimenti, A. Bolasco, M.L. Cenicola, M. D'Amico, C. Parrillo, F. Rossi, E Marmo, Anti-inflammatory, analgesic and antipyretic N-acetyl-Δ2-pyrazolines and dihydrothienocoumarines, Eur. J. Med. Chem. 27 (6) (1992) 633–639, https://doi.org/10.1016/0223-5234(92)90142-N.
[8] M.D. Altintop, A. Özdemir, Z.A. Kaplancikli, G. Turan-Zitouni, H.E. Temel, G. A. Çiftçi, Synthesis and biological evaluation of some pyrazoline derivatives bearing a dithiocarbamate moiety as new cholinesterase inhibitors, Arch Pharm 346 (3) (2013) 189–199, https://doi.org/10.1002/ardp.201200384.
[9] A. Saeed, A. Ahmed, M.B. Haider, et al., Novel pyrazoline linked acyl thiourea pharmacophores as antimicrobial, urease, amylase and α-glucosidase inhibitors: design, synthesis, SAR and molecular docking studies, RSC Adv. 14 (2) (2024) 1018–1033, https://doi.org/10.1039/d3ra06812a.
[10] R. Mehmood, A. Sadiq, R.I. Alsantali, et al., Synthesis and evaluation of 1,3,5-triaryl-2-pyrazoline derivatives as potent dual inhibitors of urease and α-glucosidase together with their cytotoxic, molecular modeling and drug-likeness studies, ACS Omega 7 (4) (2022) 3775–3795, https://doi.org/10.1021/acsomega.1c06694.
[11] V. Machado, A.R. Cenci, K.F. Teixeira, et al., Pyrazolines as potential anti-Alzheimer's agents: DFT, molecular docking, enzyme inhibition and pharmacokinetic studies, RSC Med Chem. 13 (12) (2022) 1644–1656, https://doi.org/10.1039/d2md00262k.
[12] O. Unsal-Tan, T. Tüylü Küçükkılınç, B. Ayazgök, A. Balkan, K Ozadali-Sari, Synthesis, molecular docking, and biological evaluation of novel 2-pyrazoline derivatives as multifunctional agents for the treatment of Alzheimer's disease, Medchemcomm 10 (6) (2019) 1018–1026, https://doi.org/10.1039/c9md00030e.
[13] R.J. Obaid, N. Naeem, E.U. Mughal, et al., Inhibitory potential of nitrogen, oxygen and sulfur containing heterocyclic scaffolds against acetylcholinesterase and butyrylcholinesterase, RSC Adv. 12 (31) (2022) 19764–19855, https://doi.org/10.1039/d2ra03081k.
[14] M. Taha, S. Hayat, Uddin N RahimS, A. Wadood, M. Nawaz, M. Gollapalli, A. U. Rehman, K.M. Khan, R.K Farooq, Exploring thiazole-based Schiff base analogs as potent α-glucosidase and α-amylase inhibitor: their synthesis and in-silico study, J. Mol. Struct. 1287 (5) (2023) 135672, https://doi.org/10.1016/j.molstruc.2023.135672.
[15] American Diabetes Association, Diagnosis and classification of diabetes mellitus, Diabetes Care 32 (2009) 62–67, https://doi.org/10.2337/dc09-S062.
[16] Sharma P Ritu, G.D. Gupta, V Asati, Design, synthesis and antidiabetic study of triazole clubbed indole derivatives as α-glucosidase inhibitors, Bioorg. Chem. 139 (2023) 106750, https://doi.org/10.1016/j.bioorg.2023.106750.
[17] H. Ullah, N. Nadeem, F. Rahim, A. Nawaz, A. Hussain, Synthesis, in vitro α-glucosidase, α-amylase inhibitory potential and molecular docking study of thiadiazole-sulfonamide hybrid analogues, Chem. Data Coll. 46 (2023) 101047, https://doi.org/10.1016/j.cdc.2023.101047.
[18] H. Kashtoh, K.H. Baek, New insights into the latest advancement in α-amylase inhibitors of plant origin with anti-diabetic effects, Plants 12 (16) (2023) 2944, https://doi.org/10.3390/plants12162944. Published 2023 Aug 14.
[19] S. Hayat, H. Ullah, F. Rahim, I. Ullah, M. Taha, N. Iqbal, F. Khan, M.S. Khan, S.A. A. Shah, A. Wadood, M. Sajid, A.N. Abdalla, Synthesis, biological evaluation and molecular docking study of benzimidazole derivatives as α-glucosidase inhibitors and anti-diabetes candidates, J. Mol. Struct. 1276 (2023) 134774, https://doi.org/10.1016/j.molstruc.2022.134774.
[20] A. Mushtaq, U. Azam, S. Mehreen, M.M. Naseer, Synthetic α-glucosidase inhibitors as promising anti-diabetic agents: recent developments and future challenges, Eur. J. Med. Chem. 249 (2023) 115119, https://doi.org/10.1016/j.ejmech.2023.115119.
[21] U. Ghani, Re-exploring promising α-glucosidase inhibitors for potential development into oral anti-diabetic drugs: finding needle in the haystack, Eur. J. Med. Chem. 103 (2015) 133–162, https://doi.org/10.1016/j.ejmech.2015.08.043.
[22] S. Srivastava, R. Ahmad, S.K. Khare, Alzheimer's disease and its treatment by different approaches: a review, Eur. J. Med. Chem. 216 (2021) 113320, https://doi.org/10.1016/j.ejmech.2021.113320.
[23] J.H. Shin, Dementia epidemiology fact sheet 2022, Ann. Rehabil. Med. 46 (2) (2022) 53–59, https://doi.org/10.5535/arm.22027.
[24] M. Gonçalves-Pereira, A. Verdelho, M. Prina, M.J. Marques, M. Xavier, How many people live with dementia in portugal? A discussion paper of national estimates, Port J. Public Health 39 (11) (2021) 58–68, https://doi.org/10.1159/000516503.
[25] X. Du, X. Wang, M. Geng, Alzheimer's disease hypothesis and related therapies, Transl. Neurodegener. 7 (2018) 2, https://doi.org/10.1186/s40035-018-0107-y. Published 2018 Jan 30.
[26] E.K. Perry, The cholinergic hypothesis–ten years on, Br. Med. Bull. 42 (1) (1986) 63–69, https://doi.org/10.1093/oxfordjournals.bmb.a072100.
[27] G.W. Small, P.V. Rabins, P.P. Barry, et al., Diagnosis and treatment of alzheimer disease and related disorders. consensus statement of the American Association for Geriatric Psychiatry, the Alzheimer's Association, and the American Geriatrics Society, JAMA 278 (16) (1997) 1363–1371.
[28] S. Jaipea, N. Saehlim, W. Sutcharitruk, A. Athipornchai, K. Ingkaninan, R. Saeeng, Synthesis of piperine analogues as AChE and BChE inhibitors for the treatment of Alzheimer's disease, Phytochem. Let. 53 (2023) 216–221, https://doi.org/10.1016/j.phytol.2023.01.004.
[29] R. Kandimalla, V. Thirumala, P.H. Reddy, Is alzheimer's disease a type 3 diabetes? A critical appraisal, Biochim. Biophys. Acta Mol. Basis Dis. 1863 (5) (2017) 1078–1089, https://doi.org/10.1016/j.bbadis.2016.08.018.
[30] T.T. Nguyen, Q.T.H. Ta, T.K.O. Nguyen, T.T.D. Nguyen, V.V. Giau, Type 3 diabetes and its role implications in Alzheimer's disease, Int. J. Mol. Sci. 21 (9) (2020) 3165, https://doi.org/10.3390/ijms21093165. Published 2020 Apr 30.
[31] M. Michailidis, D. Moraitou, D.A. Tata, K. Kalinderi, T. Papamitsou, V. Papaliagkas, Alzheimer's disease as type 3 diabetes: common pathophysiological mechanisms between alzheimer's disease and type 2 diabetes, Int. J. Mol. Sci. 23 (5) (2022) 2687, https://doi.org/10.3390/ijms23052687.

[32] M.V. Lourenco, S.T. Ferreira, F.G. De Felice, Neuronal stress signaling and eIF2α phosphorylation as molecular links between Alzheimer's disease and diabetes, Prog. Neurobiol. 129 (2015) 37–57, https://doi.org/10.1016/j.pneurobio.2015.03.003.
[33] B. Żyszka, M. Aniol, J. Lipok, Highly effective, regiospecific reduction of chalcone by cyanobacteria leads to the formation of dihydrochalcone: two steps towards natural sweetness, Microb. Cell Fact. 16 (2017) 136, https://doi.org/10.1186/s12934-017-0752-3.
[34] N. Kahriman, Z. Haşimoğlu, V. Serdaroğlu, F.Ş. Beriş, B. Barut, N. Yaylı, Synthesis of novel pyrazolines, their boron-fluorine complexes, and investigation of antibacterial, antioxidant, and enzyme inhibition activities, Arch Pharm 350 (2) (2017), https://doi.org/10.1002/ardp.201600285.
[35] S. Moghadam Farid, M. Noori, M. Nazari Montazer, et al., Synthesis and structure-activity relationship studies of benzimidazole-thioquinoline derivatives as α-glucosidase inhibitors, Sci. Rep. 13 (1) (2023) 4392, https://doi.org/10.1038/s41598-023-31080-2. Published 2023 Mar 16.
[36] E.U. Mughal, S. Amjid, A. Sadiq, et al., Design and synthesis of 2-amino-4,6-diarylpyrimidine derivatives as potent α-glucosidase and α-amylase inhibitors: structure-activity relationship, in vitro, QSAR, molecular docking, MD simulations and drug-likeness studies, J. Biomol. Struct. Dyn. 42 (1) (2024) 244–260, https://doi.org/10.1080/07391102.2023.2198609.
[37] F.X. Domínguez-Villa, N.A. Durán-Iturbide, J.G. Ávila-Zárraga, Synthesis, molecular docking, and in silico ADME/Tox profiling studies of new 1-aryl-5-(3-azidopropyl)indol-4-ones: potential inhibitors of SARS CoV-2 main protease, Bioorg. Chem. 106 (2021) 104497, https://doi.org/10.1016/j.bioorg.2020.104497.
[38] C.A. Lipinski, F. Lombardo, B.W. Dominy, P.J Feeney, Experimental and computational approaches to estimate solubility and permeability in drug discovery and development settings, Adv. Drug Deliv. Rev. 23 (1–3) (1997) 3–25, https://doi.org/10.1016/S0169-409X(96)00423-1.
[39] D.F. Veber, S.R. Johnson, H.Y. Cheng, B.R. Smith, K.W. Ward, K.D. Kopple, Molecular properties that influence the oral bioavailability of drug candidates, J. Med. Chem. 45 (12) (2002) 2615–2623, https://doi.org/10.1021/jm020017n.
[40] A. Daina, O. Michielin, V. Zoete, SwissADME: a free web tool to evaluate pharmacokinetics, drug-likeness and medicinal chemistry friendliness of small molecules, Sci. Rep. 7 (2017) 42717, https://doi.org/10.1038/srep42717. Published 2017 Mar 3.
[41] L.K. Williams, X. Zhang, S. Caner, et al., The amylase inhibitor montbretin A reveals a new glycosidase inhibition motif, Nat. Chem. Biol. 11 (9) (2015) 691–696, https://doi.org/10.1038/nchembio.1865.
[42] V. Roig-Zamboni, B. Cobucci-Ponzano, R. Iacono, et al., Structure of human lysosomal acid α-glucosidase-a guide for the treatment of Pompe disease, Nat. Commun. 8 (1) (2017) 1111, https://doi.org/10.1038/s41467-017-01263-3.
[43] D. Barak, C. Kronman, A. Ordentlich, N. Ariel, A. Bromberg, D. Marcus, A. Lazar, B. Velan, A. Shafferman, Acetylcholinesterase peripheral anionic site degeneracy conferred by amino acid arrays sharing a common core, J. Biol. Chem. 269 (9) (1994) 6296–6305, https://doi.org/10.1016/S0021-9258(17)37371-4.
[44] D.M. Quinn, Acetylcholinesterase: enzyme structure, reaction dynamics, and virtual transition stats, Chem. Rev. 87 (1987) 955–979, https://doi.org/10.1021/cr00081a005.
[45] P. Masson, P. Legrand, C.F. Bartels, M.T. Froment, L.M. Schopfer, O. Lockridge, Role of aspartate 70 and tryptophan 82 in binding of succinyldithiocholine to human butyrylcholinesterase, Biochemistry 36 (8) (1997) 2266–2277, https://doi.org/10.1021/bi962484a.
[46] F. Nachon, L. Ehret-Sabatier, D. Loew, C. Colas, A. van Dorsselaer, M. Goeldner, Trp82 and Tyr332 are involved in two quaternary ammonium binding domains of human butyrylcholinesterase as revealed by photoaffinity labeling with [3H]DDF, Biochemistry 37 (29) (1998) 10507–10513, https://doi.org/10.1021/bi980536l.
[47] M.J. Abraham, T. Murtola, R. Schulz, S. Pall, J.C. Smith, B. Hess, E. Lindahl, GROMACS: high performance molecular simulations through multi-level parallelism from laptops to supercomputers, SoftwareX 1 (2015) 19–25, https://doi.org/10.1016/j.softx.2015.06.001.
[48] N. Atatreh, S. Al Rawashdah, S.S. Al Neyadi, S.M. Abuhamdah, M.A Ghattas, Discovery of new butyrylcholinesterase inhibitors via structure-based virtual screening, J. Enzyme Inhib. Med. Chem. 34 (1) (2019) 1373–1379, https://doi.org/10.1080/14756366.2019.1644329.
[49] O.M. Ogunyemi, G.A. Gyebi, A. Saheed, et al., Inhibition mechanism of alpha-amylase, a diabetes target, by a steroidal pregnane and pregnane glycosides derived from Gongronema latifolium Benth, Front Mol. Biosci. 9 (2022) 866719, https://doi.org/10.3389/fmolb.2022.866719.
[50] D. Osmaniye, S. Levent, A.B. Karaduman, S. Ilgın, Y. Özkay, Z.A. Kaplancıklı, Synthesis of new benzothiazole acylhydrazones as anticancer agents, Molecules 23 (5) (2018) 1054, https://doi.org/10.3390/molecules23051054.
[51] Z. Uğraş, F. Tok, E. Şalva, G. Ultav, B. Koçyiğit-Kaymakçıoğlu, Synthesis and structural characterization of novel 2-pyrazoline derivatives: evaluation of their antiproliferative activity and fluorescence properties, Acta Pol. Pharm. 39 (5) (2022) 643–659, https://doi.org/10.32383/appdr/157503.
[52] S. Tala, H. Joshi, B. Dodiya, Synthesis and biological study of some new chalcone and pyrazole derivatives, Indian J. Chem. 52 (2018) 807–809.
[53] J.S. Kim, C.S. Kwon, K.H. Son, Inhibition of alpha-glucosidase and amylase by luteolin, a flavonoid, Biosci. Biotechnol. Biochem. 64 (11) (2000) 2458–2461, https://doi.org/10.1271/bbb.64.2458.
[54] N.V. Quan, T.D. Xuan, H.D. Tran, et al., Antioxidant, α-Amylase and α-Glucosidase Inhibitory Activities and Potential Constituents of Canarium tramdenum Bark, Molecules 24 (3) (2019) 605, https://doi.org/10.3390/molecules24030605. Published 2019 Feb 9.
[55] G.L. ELLMAN, K.D. COURTNEY, ANDRES V Jr, R.M FEATHER-STONE, A new and rapid colorimetric determination of acetylcholinesterase activity, Biochem. Pharmacol. 7 (1961) 88–95, https://doi.org/10.1016/0006-2952(61)90145-9.
[56] R. Liman, A.N. Kurşunlu, M. Özmen, S. Arslan, D. Mutlu, E.S. İstifli, Y. Açıkbaş, Synthesis of water-soluble symmetric and asymmetric pillar[5]arene derivatives: cytotoxicity, apoptosis and molecular docking studies, J. Mol. Struct. 1265 (2022) 133482, https://doi.org/10.1016/j.molstruc.2022.133482.
[57] D. Mutlu, C. Çakır, M. Öztürk, S. Arslan, Anticancer and apoptotic effects of a polysaccharide extract isolated from Lactarius chrysorrheus Fr. in HepG2 and PANC-1 cell lines, Arch. Biol. Sci. 74 (4) (2022) 315–324, https://doi.org/10.2298/ABS220803030M.
[58] G.M. Morris, R. Huey, W. Lindstrom, M.F. Sanner, R.K. Belew, D.S. Goodsell, A. J. Olson, AutoDock4 and AutoDockTools4:automated docking with selective receptor flexibility, J. Comput. Chem. 30 (16) (2009) 2785–2791, https://doi.org/10.1002/jcc.21256.
[59] E. Jurrus, D. Engel, K. Star, et al., Improvements to the APBS biomolecular solvation software suite, Protein Sci. 27 (1) (2018) 112–128, https://doi.org/10.1002/pro.3280.
[60] O.M.H. Salo-Ahen, I. Alanko, R. Bhadane, A.M.J.J. Bonvin, R.V. Honorato, S. Hossain, A.H. Juffer, A. Kabedev, M. Lahtela-Kakkonen, A.S. Larsen, et al., Molecular dynamics simulations in drug discovery and pharmaceutical development, Processes 9 (2021) 71, https://doi.org/10.3390/pr9010071.
[61] K. Vanommeslaeghe, E. Hatcher, C. Acharya, et al., CHARMM general force field: a force field for drug-like molecules compatible with the CHARMM all-atom additive biological force fields, J. Comput. Chem. 31 (4) (2010) 671–690, https://doi.org/10.1002/jcc.21367.
[62] J. Huang, A.D. MacKerell Jr., CHARMM36 all-atom additive protein force field: validation based on comparison to NMR data, J. Comput. Chem. 34 (25) (2013) 2135–2145, https://doi.org/10.1002/jcc.23354.